Journal of Hazardous Materials 491 (2025) 137691

Contents lists available at ScienceDirect

Journal of Hazardous Materials

journal homepage: www.elsevier.com/locate/jhazmat

Bioremediation of multiple heavy metals through biostimulation of microbial-induced calcite precipitation at varying calcium-to-urea concentrations

Carla Comadran-Casas [a,*], Cise Unluer [b], Adrian M. Bass [c], John Macdonald [c], Elmira Khaksar Najafi [a], Liene Spruzeniece [c], Caroline Gauchotte-Lindsay [a]

[a] Division of Infrastructure and Environment, James Watt School of Engineering, the University of Glasgow, United Kingdom
[b] Department of Civil Engineering and Management, University of Manchester, Manchester M13 9PL, United Kingdom
[c] School of Geographical & Earth Sciences, University of Glasgow, Glasgow, United Kingdom

HIGHLIGHTS

- Simultaneous carbonation of multiple heavy metals through biostimulation is evidenced.
- Urea hydrolysis and MICP removed > 85 % Pb and Zn from the exchangeable fraction.
- Increasing Ca-to-urea ratio increased carbonation of Zn, Mn, Sr and Ba.
- Heavy metal carbonation was maximised at Ca-to-urea ratio of 333:333 mM.

GRAPHICAL ABSTRACT

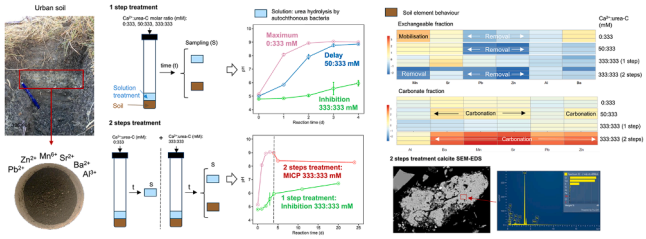

ARTICLE INFO

Keywords:
Biostimulation
MICP
Heavy metals
Soil remediation
Carbon sequestration

ABSTRACT

Studies on heavy metal bioremediation through microbial-induced calcite precipitation (MICP) typically involve bioaugmentation approaches that use low calcium-to-urea ratios and target single contaminants. We present an investigation on the efficiency of soils' autochthonous ureolytic bacteria to simultaneously remediate multiple heavy metals and sequester carbon through urea hydrolysis and MICP on an urban soil containing excess Pb, Zn, Mn, Sr, Ba and Al. Soils were treated at a fixed urea concentration of 333 mM and increasing calcium content of 0, 50 and 333 mM to provide a range of carbonation potential. Urea hydrolysis (Ca^{2+} = 0 mM) did not produce quantifiable soil carbonation and mobilised Mn into the exchangeable fraction. Ca^{2+} at 50 mM delayed soils' autochthonous ureolytic activity and produced limited carbon and heavy metal mineralisation ($CaCO_3$ = 0–0.7 %). 333 mM of Ca^{2+} inhibited urea hydrolysis however, if applied following urea hydrolysis, both carbon ($CaCO_3$ = 4–7 %) and heavy metal (Pb, Zn, Mn, Sr and Ba) mineralisation were maximised. Urea hydrolysis and MICP were most successful in removing Pb and Zn from the exchangeable fraction (>85 %). However, the higher pH induced by urea hydrolysis at Ca^{2+} = 0–50 mM (~9) compared to 333 mM (~8.5) favoured partition of Pb into the oxyhydroxide fraction. Instead, partition of Zn, Mn, Sr and Ba into the soil carbonate fraction increased with increasing calcium, whilst there was no evidence of Al carbonation. The results of this study evidence the feasibility of biostimulation approaches to remediate multiple contaminants simultaneously through MICP, provide insights into multiple element's behaviour during urea hydrolysis and MICP and demonstrate carbon and element mineralisation are maximised at equimolar calcium-to-urea ratio of 333 mM.

* Correspondence to: Advanced Research Centre, University of Glasgow, 11 Chapel Ln, Glasgow, Scotland G11 6EW, United Kingdom.
E-mail addresses: Carla.ComadranCasas@glasgow.ac.uk (C. Comadran-Casas), caroline.gauchotte-lindsay@glasgow.ac.uk (C. Gauchotte-Lindsay).

https://doi.org/10.1016/j.jhazmat.2025.137691
Received 8 November 2024; Received in revised form 3 February 2025; Accepted 19 February 2025
Available online 21 February 2025

1. Introduction

Land reclamation through the restoration of soils degraded by chemical pollution is to play a relevant role in the sustainable development of urban areas faced with development pressures. Nature-based solutions (NBS) are at the forefront of global efforts to tackle soil pollution due to their environmental, societal, and economic benefits [93]. Biological processes that result in the mineralisation of heavy metals as carbonate [1,37], struvite [94] and apatite [96,98] minerals are promising bioremediation approaches. The mineralisation of toxic elements decreases their bioavailability and thus their risk to result in harmful effects to living organisms [87].

Heavy metal biomineralisation can be driven by microorganisms such as bacteria [37] and fungi [86] and, more recently, plant-derived enzymes [72]. In particular, microbial-induced calcite precipitation (MICP) stimulates microbial activity to generate environmental conditions favouring the precipitation of carbonate minerals, i.e., abundance of carbonate ions (CO_3^{2-}) and alkaline environment of pH $\geq$ 8.5. One efficient metabolic pathway is the ammonification of urea or ureolysis. In this approach, ureolytic bacteria catalyse the hydrolysis of urea into ammonia (NH_3) and carbamic acid through the urease enzyme (Eq. 1). Carbamic acid spontaneously hydrolyses into NH_3 and carbonic acid (H_2CO_3) (Eq. 2), which subsequently equilibrate with water as bicarbonate (HCO_3^-) and ammonium (NH_4^+) ions (Eqs. 3 and 4). The excess of hydroxide (OH^-) ions between pH 6.3 and 9.3 (pK_1 and pK_a, respectively) results in a net increase in pH, in turn producing carbonate (CO_3^{2-}) ions. Given the presence of calcium (Ca^{2+}) ions, this leads to the precipitation of calcium carbonate ($CaCO_3$) minerals (Eq. 5) [39]. During $CaCO_3$ precipitation, toxic species of heavy metals (e.g., Pb^{2+}) can be mineralised through isomorphous substitution of Ca^{2+} or co-precipitate as carbonates (e.g., $PbCO_3$).

$$CO(NH_2)_2 + 2H_2O \xrightarrow{urease} NH_3 + NH_2COOH \quad (1)$$

$$NH_2COOH + H_2O \rightarrow NH_3 + H_2CO_3 \quad (2)$$

$$H_2CO_3 \leftrightarrow H^+ + HCO_3^- \quad (3)$$

$$2NH_3 + 2H^+ \leftrightarrow 2NH_4^+ + 2OH^- \quad (4)$$

$$Ca^{2+} + HCO_3^- + OH^- \leftrightarrow CaCO_3 + H_2O \quad (5)$$

Ca^{2+} ions play a relevant role in several aspects that affect the efficiency of heavy metal bioremediation via MICP. Ca^{2+} has been found to favour microbial activity by decreasing the sorption of heavy metals onto the cell [14,34]. However, Ca^{2+} has also been shown to hinder microbial activity by increasing toxic element concentration through exchange with heavy metals adsorbed on the soil matrix [24]. Ca^{2+} contributes to determining the extent of soil carbonation, which directly affects soil mechanical properties (e.g., permeability, shear strength, liquefaction) [29,8] and could prove desirable in urban settings. Furthermore, Ca^{2+} affects the extent and mechanism of carbon sequestration and storage (CCS). MICP results in atmospheric and urea derived CCS through mineral and solubility trapping [70,75,76,25]. Absence of Ca^{2+} results in solubility trapping whilst its presence facilitates mineral trapping, which is a more stable and desirable form of CCS in the current context of climate change [25]. Bioremediation studies typically use low calcium-to-urea molar ratios (25:333 mM) that are sufficient for the carbonation of toxic elements [3,6,2,23,58,59,99,107] but limit enhancement of soil mechanical properties [7] and CCS [26]. Varying calcium-to-urea ratios may result in differing bioremediation efficiencies and CCS mechanisms, leading to variations in carbonate products and heavy metal immobilisation efficiencies.

MICP consistently shows high heavy metal bioremediation efficiency in soils. Removal of > 97 % Cr^{6+} [21,5,58,59], 97 % As^{3+} [3], 26–86 % Pb^{2+} [99,6,41,65], 80 % Sr^{2+} [2], 13–88 % Cd^{2+} [41,65], 96 % Ni^{2+} [107], 92–97 % Cu^{2+} [23,41] and 21–66 % Zn^{2+} [65] from the soil soluble/exchangeable fraction are accompanied by respective increases in the carbonate-bound fraction. Most research, however, has been conducted on bioaugmentation, which may have several potential drawbacks (e.g., higher treatment costs, predation of bacteria, homogeneity of bacteria inoculation, limited to culturable bacteria). Biostimulation offers several advantages. It avoids the necessity of culturing and inoculating bacteria, potentially reducing treatment complexity and costs. Through their natural distribution and ubiquitousness [19], autochthonous ureolytic bacteria act ad hoc and may be better adapted to the polluted environment. Additionally, biostimulation targets the overall ureolytic consortium instead of culturable bacteria, which estimated proportion of the total soil bacterial population is low (est. <1 %) [101]. Chen and Achal [23] and Lyu et al. [67] showed carbonation of Cu^{2+} and Cd^{2+} through biostimulation, evidencing its plausibility as a bioremediation approach. Bioremediation via MICP on soils affected by multiple contaminants however is still scarce [99,41,65] and, to our knowledge, limited to bioaugmentation. In presence of multiple toxic elements, element atomic radii and valence could play a role in the specificity for element carbonation [44] and result in differing bioremediation efficiencies across elements.

The current state of art highlights the need to advance knowledge on the bioremediation efficiency of MICP through biostimulation in the presence of multiple toxic elements. Furthermore, there is a need to evaluate different heavy metal immobilisation mechanisms and explore the potential to maximise additional ecosystem services (e.g., soil stabilisation, carbon sequestration). Here we present an investigation on the effect of varying calcium-to-urea molar ratios on the bioremediation efficiency and soil carbonation with the aim of identifying a treatment that maximises both. The focus of the study was a silty sand from an urban area with excess Pb, Zn, Ba, Mn, Sr and Al compared to regional levels. The first goal was to determine whether MICP through biostimulation could be induced in the presence of multiple toxic elements. The second goal was to assess the bioremediation efficiency under varying calcium-to-urea molar ratios to maximise concomitant heavy metal and carbon sequestration through mineral trapping. We hypothesised an increased bioremediation efficiency and carbon sequestration through mineral trapping with increasing Ca^{2+} content. The results provided scientific evidence for the suitability of biostimulation of autochthonous ureolytic bacteria for the maximisation of simultaneous bioremediation of multiple toxic elements and CCS through mineral trapping.

2. Materials and methods

2.1. Soil sampling

The soils used in this study comprised two sandy soils from quarries and a soil from a vacant and derelict land site in Glasgow (UK) (Fig. 1). Reddish and yellow sand samples were sourced from Garnock (GQ) and Hullerhill (HQ) quarries, respectively, operated by Hugh King & Co and located in Ayrshire, Scotland (UK) (GQ: 55.63757713, −4.718350936; HQ: 55.66784963, −4.66816856; WGS84). The soil sample from the vacant and derelict site (GLA) was obtained from Glenconner Park (Glasgow, Scotland, UK, Figure S1). The top ~40 cm soil profile revealed a top organic layer of soil overlaying a brown/reddish clay layer (Figure S1). An interbedded layer of made ground was sampled. It consisted of non-cohesive granular material of sandy to gravelly texture with fines and of light to dark colour. Bricks and unidentified rubble were appreciable. Once in the laboratory, soil samples were sieved <2 mm in sterile conditions and stored in a cooled room at 4 °C until further use. A subsample from each soil was analysed for particle size distribution, total carbon, total and exchangeable elemental composition and mineralogy as specified in Section 2.5.

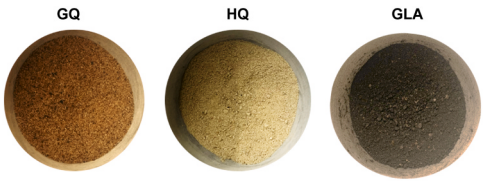

Fig. 1. Reddish sand from Garnock quarry (GQ), yellow sand from Hullerhill quarry (HQ), Ayrshire, and sandy soil from vacant and derelict land site in Glenconner park, Glasgow, (GLA).

2.2. Treatment solutions

Treatment solutions contained 333 mM urea (Fisher Scientific, ≥99.5 % ACS reagent), 10 g/L ammonium chloride (NH_4Cl, VWR Chemicals, ≥99.9 % ACS reagent), 3 g/L nutrient broth (Sigma Aldrich) and either 0-, 50-, or 333-mM calcium chloride dihydrate ($CaCl_2 \bullet 2\ H_2O$, Sigma Aldric, ≥99 % ACS reagent) in deionised water (Milli-Q water filtration system Elga Purelab Chorus). $CaCl_2$ was used to induce higher urease activity and calcite precipitation over other calcium sources [4]. A control with no added calcium was chosen to study the potential carbonation of heavy metals through urea hydrolysis. Ca^{2+} concentrations of 50 and 333 mM Ca^{2+} were representative of MICP applications in bioremediation (e.g., [3,23]) and geotechnical engineering [7], respectively. Control treatments were equally prepared but excluded urea. Stock solutions were filter sterilised through sterile 0.2 µm syringe filters (Sartorius Minisart), transferred into pre-autoclaved glass bottles in sterile conditions and stored at 4ºC until further use.

2.3. Application of MICP treatments

Samples were prepared by adding 2 g of soil (<2 mm) in sterile DNA, DNAse, and RNAse free15 mL centrifuge tubes (Sarstedt AG&Co KG). Following preparation, 4 mL treatment solution was pipetted, tubes were closed and thoroughly shaken to mix soil and solution, which marked $t = 0$. Treatment was applied at a 1:2 soil-solution ratio as in Achal et al. [3], Achal et al. [2] and Yang et al. [99]. This ensured submerged conditions and therefore access to reactants, whilst ensuring sufficient volume for post-treatment sampling and analysis. Both sample preparation and treatment application were conducted in sterile conditions. Samples were subsequently transferred into an orbital shaker incubator set at standard laboratory temperature (20 ± 3 ºC) and gentle shaking (150 rpm) and allowed to react in closed vials and dark conditions.

MICP treatments comprised one stage treatments, where treatment solution was applied once, and two stage treatments, where treatment solution replacement occurred once after a certain reaction time. One stage treatments comprised: urea with 0 mM Ca^{2+} (U); urea with 50 mM Ca^{2+} (U LCa); urea with 333 mM Ca^{2+} (U HCa); and their respective controls without urea: C, C LCa, C HCa. Samples were taken at reaction time points (t_r) 1 h, 1, 2, 3 and 4 d. For samples that received urea in which no significant increase in solution pH was observed within this time period (indicative of no ureolysis), reaction time was extended up to 20 d.

Two-stage treatments comprised treatment cases containing high calcium, i.e., urea with 333 mM Ca^{2+} (U HCa 2S) and its respective control (C HCa 2S). For these two treatments, an initial application of 4 mL of either U or C treatment solution was allowed to react for $t_r = 4$ d. This was followed by solution replacement and application of 4 mL of either U HCa or C HCa treatment solution, which was allowed to react for $t_r = 1$ d, for a total treatment time of 5 d. To replace the treatment solution, samples were centrifuged at 5000 rpm for 20 min. Then, in sterile conditions, the supernatant was decanted, and fresh treatment solution was pipetted as previously detailed. Sampling was destructive and three replicate samples were prepared for each time point and treatment.

2.4. Post-treatment sampling

Following reaction time, 15 mL tubes containing soil and treatment solution were centrifuged at 5000 rpm for 20 min. This centrifugation speed and time promotes pelleting of bacteria and therefore prevents presence of bacteria in the supernatant. In sterile conditions, the supernatant was decanted, filtered through sterile 0.2 µm syringe filters, transferred into 2 mL pre-autoclaved centrifuge tubes, and subsequently stored at −20 ºC until analysis of solution pH and NH_4^+ (see Section 2.5.1 and 2.5.2). The remaining soil samples were stored at −20 ºC for post-treatment geochemical characterisation. In preparation for geochemical analyses, soil samples were oven dried at 70 ºC to a constant mass. Soil sample replicates were gently homogenised with a pestle and mortar to produce a composite sample. Three 1 g subsamples were then obtained for sequential extraction of heavy metals (see Section 2.5.5). The remaining composite sample was ground and sieved <50 µm in preparation for XRD and TG analyses (see Sections 2.5.6 and 2.5.7, respectively).

2.5. Physicochemical analyses

2.5.1. pH

Solution pH was analysed with a pH meter (Orion Star A215, Thermo Scientific) probe (Orion ROSS Ultra SM 103BNUWP, Thermo Scientific), calibrated to three points (pH = 4, 7 and 10, Orion Application Solution, Thermo Scientific).

2.5.2. NH_4^+

Ammonium in solution was analysed with an ammonium cuvette test (100–1800 mg/L NH_4-N, LCK502, Hach UK) with a spectrophotometer (DR 1900, Hach UK) on three sample replicates.

2.5.3. Particle size distribution

Soil samples were oven dried at 105 ºC to a constant mass and subsequently pre-treated with hydrogen peroxide on a hot plate at 90 °C to remove soil organic matter. The particle size distribution (PSD) of the mineral soil fraction was analysed on three replicate samples with a laser diffractometer (Bettersize 2600 Laser Particle Analyzer, BT-802, Bettersize Instruments Ltd.).

2.5.4. Soil total carbon

Soil total carbon of three replicate samples were analysed with a Picarro Combustion Module Cavity Ring-Down Spectroscopy (CM-CRDS) system (CM by NC Technologies, G2201-i CDRS) interfaced by a Caddy Continuous Flow Interface (A2100).

2.5.5. Soil elemental composition and heavy metal partition into soil fractions

The total elemental composition of the three untreated soils was carried out through a triacid hotplate digestion at the Scottish University Environment Research Centre (SUERC, East Kilbride, G75 0QF, Scotland, UK) in triplicate. Soil samples were consecutively digested overnight on a hotplate at 120º, first with $HF+HNO_3$, secondly with HNO_3 and finally with HCl. Elements Al, Ba, Ca, Fe, K, Mg, Mn, Na, Sr, Ti and Zn were determined by inductively coupled plasma-optical emission spectrometry (ICP-OES, Thermo Scientific iCap 7000) and As, B, Cd, Co, Cr, Cu, Li, Mo, Ni, Pb, Sb, Sn and V by ICP-mass spectrometry (ICP-MS, Agilent 7500ce). ICP-MS was used due to the higher limit of detection over ICP-OES according to SUERC internal laboratory procedures.

The element partition into soil exchangeable, carbonate, organic matter, oxyhydroxide and residual fractions was determined through sequential extraction [91]. The exchangeable and carbonate extraction steps were conducted on all treated samples obtained after $t_r = 1$ h, 1, 4 and 5 d. The organic matter, oxyhydroxide and residual extraction steps

were only conducted on samples treated with the U treatment at $t_r = 1$ h, and samples treated with U HCa and U LCa at $t_r = 4$ d. The residual fraction was conducted though a triacid digestion at SUERC as previously described. Elements Na, K, Mg, Ca, Sr, Ba, Ti, V, Cr, Mo, Mn, Fe, Co, Ni, Cu, Zn, Cd, B, Al, Si, Sn, Pb, As, Sb, S, Se on samples obtained from extraction steps 1–4 were determined by ICP-OES (Agilent 5900 SVDV). Samples obtained after extraction step 5 were determined by ICP-OES or ICP-mass at SUERC as indicated previously.

2.5.6. Powder X-ray diffraction (XRD)

The mineralogy of ground (<50 μm) soil samples was analysed by powder X-ray diffraction. X-ray diffraction patterns were collected at ambient temperature on a Malvern Panalytical Empyrean with PIXcel3D-Medipix3 1 × 1 detector using Cu Kα radiation (wavelength 1.541874 (Å)). Data were collected in Bragg-Brentano reflection geometry 5–80° 2θ, step size 0.0131°. Data analysis was carried out with the HighScore Plus software (version 5.1a 5.1.1.30138, Malvern Panalytical B.V., Almelo, the Netherlands). Rietveld refinement was used to quantify soil mineralogy.

2.5.7. Thermogravimetric analysis (TG)

The thermal decomposition of soil samples collected at $t_r = 1$ h, 1, 4 and 5 d and chemicals used in treatment solutions (i.e., urea, calcium chloride dihydrate, nutrient broth and ammonium chloride) were analysed with a thermogravimetric analyser (TGA 8000, PerkinElmer). Samples of 10–15 mg weight were heated from 30 to 1100 °C at a rate of 10 °C/min. N_2 was used as a carrier gas, with sample and balance purges set to 40 and 60 mL/min, respectively. Data analysis was carried out with the Pyris software (Pyris™ V13.4.0, PerkinElmer).

2.5.8. Attenuated total reflectance-fourier transform infrared spectroscopy (ATR-FTIR)

Ground soil samples collected at $t_r = 1$ h, 4 and 5 d were analysed by ATR-FTIR (Spectrum 3, PerkinElmer). Background and samples spectra were collected over the wavenumber range 4000–600 cm^{-1} with a resolution of 4 cm^{-1}. Results are the average of 32 scans. Base correction and peak identification were performed using the software Spectragryph (v1.2.16.1).

2.5.9. Scanning electron microscopy-electron dispersive X-ray spectroscopy (SEM-EDS)

Ground soil samples collected at $t_r = 4$ and 5 d were analysed by scanning electron microscope (SEM) coupled with energy-dispersive spectroscopy (EDS). SEM-EDS was used to determine morphology and elemental composition of precipitated calcium carbonate grains. Sample imaging and chemical mapping was conducted on polished epoxy mounts with a ca 20 nm carbon coating to avoid charging. Analysis was performed with a variable pressure field-emission-gun scanning electron microscope (Zeiss Sigma VP-FEGSEM) equipped with an energy dispersive detector (170 mm^2 Silicon Drift Detector Ultim Max, Oxford Instruments). The analysis was conducted in high vacuum using high current mode, aperture 60 μm at working distance of 8.0 mm. The secondary electron (SE), backscatter (BSE) images and EDX maps were acquired using accelerating voltage of 10 kV in order to maximize the higher spatial resolution for illustrating the fine scale of the porosity and inclusion sizes. The EDS spectra was obtained using accelerating voltage of 20 kV to excite the X-ray lines of heavy elements (such as Pb), which could not be detected with 10 kV accelerating voltages. EDS data were acquired and processed using the Oxford Instrument AZtec 6.1 software.

2.6. Data analysis

The statistical programming language R and Rstudio (v. 4.2.2) [95, 28,82,85] was used to compute average and standard deviation of replicate samples (e.g., pH, PSD, TOC) and analyse the data derived from the sequential extraction. A non-targeted hierarchical cluster analysis (HCA) was used to elucidate similarities in elements behaviour caused by treatment and reaction time in the soil exchangeable and carbonate fractions. The R packages 'dendextend', 'factoextra', 'cluster', 'pheatmap' and 'NbClust' were used for HCA.

The element concentrations from the sequential extraction at t_{end} were normalised with respect to samples treated with control treatment (C) at t_0 ($t_r = 1$ h) to remove the effect of applied chemicals other than urea and $CaCl_2$. The normalised averages and error propagated during normalisation at t_0 and t_{end} for each element were computed as [57]:

$$t = 0 \quad E_{n,0} = \frac{E_{0,av}}{E_{0,av}}\left(1 \pm \sqrt{2}\ \frac{E_{0,sd}}{E_{0,av}}\right) = 1 \pm \sqrt{2}\ \frac{E_{0,sd}}{E_{0,av}} \tag{6}$$

$$t = end \quad E_{n,f} = 1 - \frac{E_{f,av}}{E_{0,av}}\left(1 \pm \sqrt{\left(\frac{E_{0,sd}}{E_{0,av}}\right)^2 + \left(\frac{E_{f,sd}}{E_{f,av}}\right)^2}\right) \tag{7}$$

Where $E_{n,0}$ and $E_{n,f}$ are the normalised average concentrations of element 'E' and subscript '0' and 'f' indicate reaction time t_0 and t_{end}, respectively. $E_{0,av}$ and $E_{f,av}$ are average element concentrations and $E_{0,sd}$ and $E_{f,sd}$ their respective standard deviations. Note the normalised element concentration at t_{end} is computed as one minus fraction, therefore positive results indicate removal and negative results relative increases. Scripts are available upon request.

3. Results and discussion

3.1. Pre-treatment soils characterisation

The particle size distribution indicated the GQ and HQ quarry soils were composed of 100 % and 90 % sand, respectively (Figure S 2 and Table S 1). The yellow sand (HQ) contained ~9 % fines (<63 μm), of which ~2 % were of clay size (<2 μm). XRD analysis indicated the main mineral constituents of the GQ soil were quartz (88 %) and albite (8.1 %), with traces of dolomite, microcline, and enstatite (Table S 4). The HQ soil contained quartz (91 %) and kaolinite (8.4 %) and traces of muscovite (Table S 5). The GLA soil was a silty sand, with ~31 % fines of which <5 % were of clay size. The GLA soil mineralogy was quartz (54 %), mullite (24 %) and bytownite (20 %) with traces of birnessite (Table S 6). HQ and GQ soils contained no quantifiable carbon whilst the total carbon in GLA soil samples was determined at 3 % (Table S 2). XRD analysis indicated no detectable calcite in any of the soils prior to treatment (Table S 4, 5 and 6).

Total elemental analysis indicated the GQ soil contained Ba, Cr, Cu, Mn, Ni, Pb, Sr, V and Zn <50 mg/kg and As, Cd, Co, Mo, Sb, B, Li and Sn < 10 mg/kg. The HQ soil showed the same results except for Ba and Mn which were 50–100 mg/kg. The GLA soil contained a significantly higher content of Ba, Mn, Sr and V (>300 mg/kg), Ni and Pb (>200 mg/kg), Cr, Cu and Zn (≥100 mg/kg), Co, Li and As (20–60 mg/kg) and a similar concentration of Cd, Mo, Sb, B and Sn (≤10 mg/kg) (Figure S 3). The main elements in the exchangeable fraction of GLA soil were Al, Ba, Mn, Pb and Zn, determined between 9 to 35 mg/kg, whilst in HQ and GQ soils were <5 mg/kg (Figure S 4a). The rest of elements analysed (As, Cd, Co, Cu, Cr, Mo, Ni, Sb, V) were in trace concentrations (<2 mg/kg) in all three soils (Figure S 4b). Elements in the exchangeable fraction of HQ and GQ soils were present in trace concentrations or below limit of detection. Hence, these soils were considered "uncontaminated", being adequate controls for the study, and sequential extraction was not conducted.

3.2. Activity of soil autochthonous ureolytic microorganisms

Control soils GQ and HQ and GLA soil with excess Pb, Zn, Ba, Sr, Mn and Al were treated at varying urea-to-calcium ratios to investigate biostimulation of MICP. Soil-solution pH was used as a proxy to monitor the activity of soils' autochthonous ureolytic microorganisms. pH has been routinely used to evidence urea hydrolysis in bioremediation

studies in inoculated solutions [9,12,14,31,36,37,44,53,73,97], soils [105,24,67], mine tailings [99,100,74,78] and sludge [104]. pH is a suitable parameter as it is indicative of urea hydrolysis and favourable conditions for soil carbonation (pH >8.5). In MICP, increases in soil solution pH via urea hydrolysis occur as a result of urea derived NH_3 protonation to NH_4^+, which generates excess OH^- according to Eqs. (3) and (4). This is favoured up to pH circa 9 when pH is buffered due to deprotonation of NH_4^+ to NH_3 ($pK_a = 9.26$) and HCO_3^- to CO_3^{2-} ($pK_a = 10.34$).

The application of treatments containing urea and Ca^{2+} ≤50 mM (U, U LCa) to HQ, GQ and GLA soils resulted in increases in soil solution pH to 9 within 2 to 3 days (Fig. 2a-c). This differed from pH observed in control treatments (C, C LCa) which remained < 7. The increase in pH observed in U and U LCa treatments was consistent with urea hydrolysis reactions and pH increases reported in the literature, indicating successful biostimulation of urea hydrolysis by soils' autochthonous ureolytic bacteria. This was confirmed by NH_4^+ concentrations in the solution of U samples, which indicated that all urea had been hydrolysed by day 4 (Fig. 2a-c).

With the application of urea and no calcium (U), the GLA and GQ soils showed a faster increase in soil-solution pH compared to the HQ soil. This could be related to the presence of kaolinite clay present in HQ. Clay particles can adsorb OH^- ions onto surface positively charged sites [30], buffering changes in soil-solution pH. Bacteria interact physically and chemically with clay particles due to their similar size (bacteria: 0.5–3 μm; clay: ≤2 μm) and surface electrical charges. As a result, their metabolic activity can be adversely affected by clays [20,71]. Clays can adsorb extracellular enzymes, resulting in slower bulk reaction rates [40]. Additionally, urease activity will differ significantly across local microorganisms [55] therefore different soil microbial consortia may result in different bulk urea hydrolysis rates.

With the addition of 50 mM Ca^{2+} (U LCa) increase in soil pH circa 9 was delayed up to 24 h and stabilised at a slightly lower pH (8.8–9) compared to the U treatment (9–9.1) (Fig. 2a-c). These effects were more pronounced in the HQ and GLA soils than in GQ. Similarly, autochthonous ureolytic microorganisms exhibited slower urea hydrolysis rates when exposed to urea plus calcium compared to solely urea in a Cd-seleniferous soil (Cd ~ 10 mg/kg) [67]. With the addition of 333 mM Ca^{2+} (U HCa), no notable increase in pH could be observed within 4 d, indicating limited urea hydrolysis. This was consistently observed across the three soils (Fig. 2a-c) and sustained for at least 20 d (GLA, Fig. 2d; HQ and GQ, Figure S 6). These results indicated a negative effect of Ca^{2+} on urea hydrolysis and favourable conditions for carbonation were not achieved with U HCa. NH_4^+ measurements on U HCa samples corroborated limited urea hydrolysis on GQ and HQ soils and no urea hydrolysis on GLA soil on day 4 (Fig. 2a-c).

Negative effects of Ca^{2+} on urea hydrolysis are considered to occur due to osmotic stress caused by increased salinity and coating of cell surfaces by Ca^{2+} [35]. In pure cultures of *S. pasteurii*, negative effects on urea hydrolysis were observed at Ca^{2+} >10 mM leading to complete inhibition at 200 mM [27]. Ca^{2+} ions accumulating on the negatively charged cell surfaces offer a protection mechanism to the cell against toxic elements at low Ca^{2+} (≤5 mM) [96,98]. However, at high 333 mM Ca^{2+}, cell encapsulation by $CaCO_3$ precipitated on the cell surface at early stages of urea hydrolysis prevents the cell to further access the substrate, resulting in urea hydrolysis inhibition [102]. The encapsulation phenomenon however can be prevented at high initial cell concentrations, as shown in bioaugmentation studies where urea hydrolysis by *S. pasteurii* has been observed at concentrations of up to 1 M $CaCl_2$ [7].

Urea hydrolysis inhibition by monovalent and divalent elements other than Ca^{2+} may have also contributed to the observed results. The

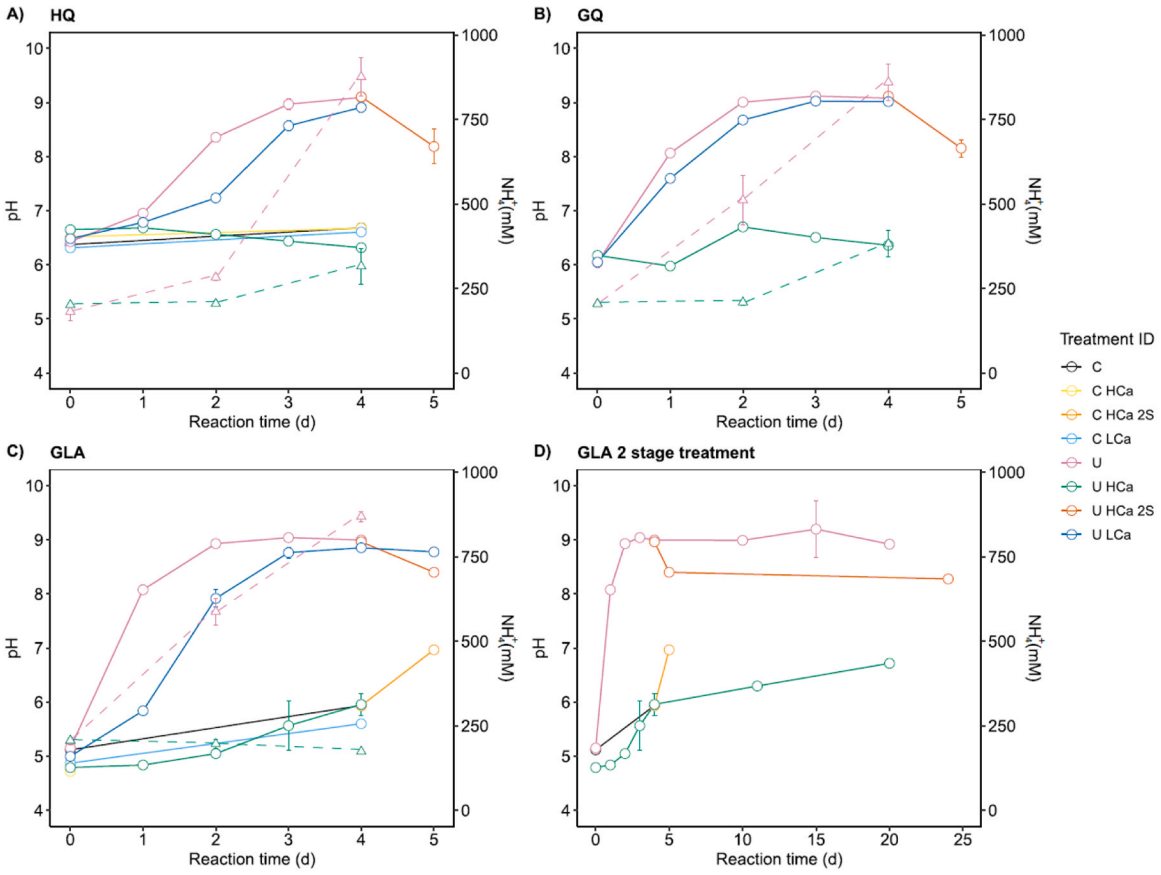

Fig. 2. pH (left y-axis, solid line) and NH_4 (mM, right y-axis, dashed line) of soil leachates of quarry sands (HQ and GQ) and VDL site soil (GLA) silty sand as a function of reaction time for various soil treatments. Markers and error bars indicate average and standard deviation, respectively, of three replicate samples.

reported strength of soil bulk ureolysis inhibition at 5 μmol/g follows $Ag^{+} \geq Hg^{2+} > Cu^{2+} > Cd^{2+} > Zn^{2+} > Sn^{2+} > Mn^{2+}$ and additional inhibition was observed with Ni^{2+}, Co^{2+}, Pb^{2+}, Ba^{2+}, As^{3+}, Cr^{3+}, Al^{3+}, V^{4+} and Mo^{6+} [90]. The total concentration of the main elements found in the exchangeable fraction of the GLA soil (Pb, Zn, Mn, Sr, Ba and Al) was of 1.38 μmol/g. Hence, a level of inhibition by Pb, Zn, Ba, Sr, Mn and Al in this soil was conceivable. This could have been exacerbated by exchange of applied Ca^{2+} with toxic elements adsorbed on the soil matrix. In *S. pasteurii*, the decrease in urea hydrolysis with increasing Ca^{2+} in a Cu-spiked soil was attributed to Cu-induced toxicity, as the Cu concentration in solution increased linearly with Ca^{2+} application up to 450 mM [24]. Similarly, we determined an initial increase in soluble Cu^{2+} (from 0.01 to 0.027 mM) and additionally Mn, Sr, and Co with the application of 333 mM Ca^{2+} (U HCa) compared to control (C) treatment at $t_r = 1$ h (Figure S 8). The increase in the concentration of these elements at t_0 thus may have increased toxicity and contributed to the observed urea hydrolysis inhibition. However, elements in the exchangeable fraction prior to treatment were determined at lower concentrations than reported minimum inhibitory concentrations (MIC) of different ureolytic bacteria species (Table 1). Furthermore, urea hydrolysis inhibition at 333 mM Ca^{2+} was also observed in HQ and GQ soils, which contained insignificant concentrations of toxic elements. Differences in the time required to increase soil pH to ~9 between HQ and GQ soils and the GLA soil were not significantly different at 50 mM Ca^{2+} (Fig. 2a-c). This suggested that elements present at the concentrations determined, nor their combined effect, had a notable negative impact on urea hydrolysis. The observed delay to inhibition of urea hydrolysis with application of 50 and 333 mM Ca^{2+} was hence largely attributed to an encapsulation of cells by $CaCO_3$ at early stages of urea hydrolysis, preventing further urea hydrolysis and therefore increases in pH.

Urea hydrolysis inhibition by 333 mM Ca^{+} was circumvented with a two-step treatment. Application of 333 mM Ca^{2+} following 4 days of urea hydrolysis resulted in an increase in pH from 5 to 9 on day 4 followed by a decrease to 8–8.5 on day 5 (U HCa 2S, Fig. 2d).This was reproducible on GQ and HQ soils (Figure S 6). pH then remained stable up to 20 days. With availability of Ca^{2+} and CO_3^{2-} ions and a pH > 8.5, precipitation of $CaCO_3$ occurs according to Eq. (5). The observed decrease in pH from day 4 to 5 was consistent with pH evolution during MICP and indicative of $CaCO_3$ precipitation [32].

In the corresponding control treatment (C HCa 2S), an increase in pH occurred following application of 333 mM Ca^{2+}, which remained ≤ 7. Data for this treatment was not collected for reaction times >5 d therefore we could not observe the evolution up to $t_r = 20$ d. The observed increase in pH with C HCa 2S was attributed to the applied salts. $CaCl_2$ and NH_4Cl application typically decreases soil solution pH [52,54,77,89] due to a variable charge mechanism of Ca^{2+} exchange with H^{+} and Al^{3+} adsorbed to organic matter and/or clays [11,89]. In the context of MICP, a decrease in pH with salt application has been observed by Lyu et al. [67]. In highly weathered acidic soils with low organic matter content, however, Cl^{-} exchange for OH^{-} adsorbed to colloid surfaces can exceed Ca^{2+} exchange with H^{+} and Al^{3+}, increasing pH [89]. This possibly explained the increase in soil pH following $CaCl_2$ application in this study. This phenomenon has also been observed on an acidic soil of similar initial acidic pH (pH = 5.3) [62].

3.3. Effect of Ca^{2+} on soil carbonation

Following successful biostimulation of urea hydrolysis by autochthonous bacteria on the three studied soils, analytical techniques were employed to elucidate presence and quantity of carbonated products and immobilisation of heavy metals.

3.3.1. XRD analysis

Mineralogical analysis of crystalline components by XRD in GLA soil samples indicated nearly identical patterns for control samples (C, C LCa, C HCa 2S) and samples that received urea and urea-high calcium (U and U HCa) treatments (Fig. 3a). No differences in soil mineralogy were detectable between these samples at reaction times t_0 and t_{end}. Some variability in peak intensities observable between $2\theta = 27$ to 28.5 was attributed to small changes in plagioclase content. These results confirmed that control treatments (excluding or including calcium) and treatments that inhibited urea hydrolysis due to the high calcium dose did not result in quantifiable soil carbonation nor other changes in soil mineralogy.

No indication of carbonate products was detectable in samples that underwent urea hydrolysis only (U). U LCa samples showed an increased peak intensity that coincided with the main peak of calcite ($2\theta = 29.43$) (Fig. 3b). However, the other calcite peaks were hardly observable (Fig. 3a) thus identification of calcium carbonate was inconclusive. The formation of Pb, Zn, Cu, Cd, Ni, and Co carbonate minerals during urea hydrolysis is possible [106,49,50,60,61,81]. However, in the presence of calcium, Pb, Zn, and Cd are reported to incorporate into calcite instead, except for Sr, which forms a soil-solution phase of calcian-strontianite [99,6,37,41,53,74]. Element carbonation may have occurred with the U and U LCa treatments. The low concentration of divalent elements, however, may have produced carbonation levels below limit of detection of powder XRD analysis (0.1–1 %).

The application of U HCa 2S treatment to GLA soil samples resulted in two new mineral phases, identified as calcite and salammoniac ("▼" and "◇" in Fig. 3, respectively). Calcite peaks were determined at 2θ equal to 29.43, 48.52, 47.50, 43.15, and 23.10. Other calcium carbonate polymorphs (aragonite, vaterite) were not detectable. Similarly, calcite has been reported as the main carbonate mineral following MICP bioaugmentation on a Pb-contaminated soil [6] and mine tailings [99,41]. Vaterite and aragonite, however, have also been identified [6,41]. Salammoniac, or ammonium chloride, is a soft halide mineral with formula NH_4Cl, soluble in water (39.5 g/100 g water at 25 ºC) [43]. Its precipitation with the U HCa 2S treatment was attributed to additional Cl^{-} from high $CaCl_2$ dose and excess NH_4^{+} derived from urea hydrolysis to the already applied NH_4Cl. Evidence of ammonium-based minerals was reported by Govarthanan et al. [41] and Yang et al. [99], who identified

Table 1
Minimum inhibitory concentration (MIC) of heavy metals on urea hydrolysis by some elements reported in the literature and present in the GLA soil. LoQ stands for limit of quantification calculated as three times the limit of detection of each element.

Element	Literature			Soils used in this study		
	MIC (mM)	Microorganism	Ref.	GQ(μM)	HQ(μM)	GLA(mM)
Pb	0.01−0.5	*Pararhodobacter sp.*	Mwandira et al. [74]	<LoQ	<LoQ	0.08 ± 0.003
	0.97−1.45	*Bacillus sp. JX910224*	Govarthanan et al. [41]	(0.01)	(0.01)	
	1−30	*S. pasteurii*	Mugwar and Harbottle [73]; Jiang et al. [48]			
	100	*E. cloacae* KJ−46 and KJ−47	Kang et al. [50]			
Zn	0.2−0.5	*S. pasteurii*	Mugwar and Harbottle [73]	<LoQ	4 ± 0.6	0.13 ± 0.003
	2.29−3.06	*Bacillus sp. JX910224*	Govarthanan et al. [41]	(0.006)		
	0.92	*Sporosarcina* kp−4 and kp−22	Qiao et al. [81]			
Mn	< 50	*S. pasteurii*	Fang et al. [34]	1 ± 0.6	8 ± 0.5	0.18 ± 0.01
Sr	2.5−5	*Halomonas sp.*	Achal et al. [2]	7 ± 0.6	3 ± 0.07	0.08 ± 0.002

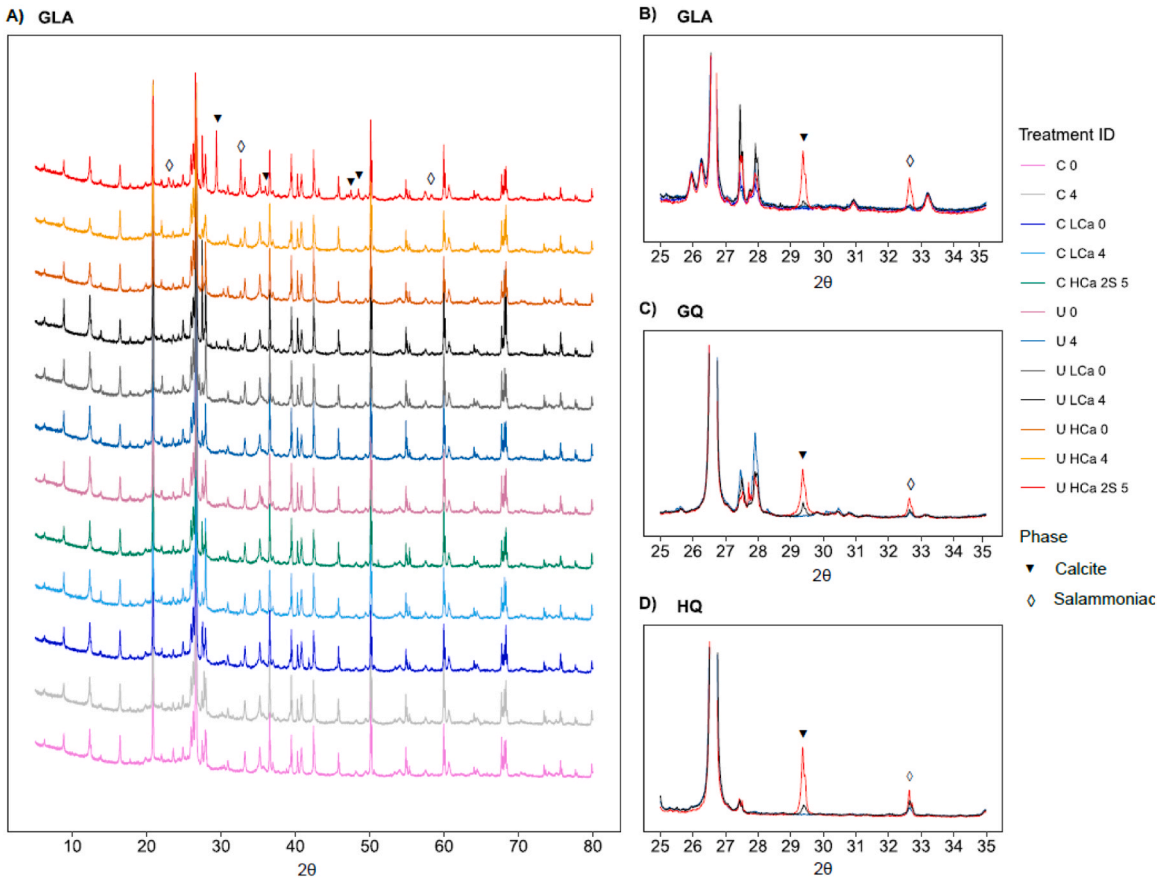

Fig. 3. XRD analysis of samples following biostimulation of MICP on a-b) GLA, c) GQ and d) HQ soils. Legend indicates treatment ID (C, C HCa 2S, C LCa, U, U HCa, U HCa 2S, U LCa) and reaction time ("0", "4", "5" refer to t_r = 1 h, 4 and 5 d, respectively). Within plots, symbols indicate the main peaks of calcite [RRUFFID=R050128] (▼) and salammoniac (◊) [RRUFFID=R050128].

gwihabaite, $(NH_4,K)NO_3$, following MICP treatment.

The observed results in GLA soil were reproducible in GQ and HQ soils. Contrary to GLA, however, increases in calcite peak intensities were unequivocally detectable with the U LCa treatment. This could be attributed to the higher cation exchange capacity of GLA soil compared to HQ and GQ soils, due to its higher fines content (26 %) and organic carbon content (3 %). The adsorption of applied Ca^{2+} may have reduced its availability for carbonation at the low Ca^{2+} dosage (50 mM), leading to insignificant carbonation in GLA.

The estimated calcite content from Rietveld analysis in GLA, GQ and HQ with U HCa 2S treatment were 6.9, 3.1 and 4.6 %, respectively. The U LCa treatment resulted in 0.5 % calcite in GQ and HQ. These results further confirmed successful MICP by autochthonous indigenous microorganisms on the three soils studied and demonstrated soil carbonation was maximised with the U HCa 2S treatment. The results are constrained by the detection limits of the XRD instrument used. Higher-resolution XRD analysis could help determine whether carbonate precipitation or other mineral phases occurred at 50 or 0 mM Ca_2^+.

3.3.2. *Thermal decomposition of soils (TG)*

Samples of GLA soil that received control treatments decomposed in four main stages: 1) 30–120 °C; 2) 120–390 °C; 3) 390–750 °C and 4) 750–1100 °C (Fig. 4a-c) during TG analysis. The first decomposition stage corresponded to adsorbed water. The main decomposition peaks (235–238°C and 286–315°C) during the second stage coincided with those of nutrient broth and ammonium chloride (Table S 7 and Figure S 8). Mass loss peak during the third stage (477 ± 5 °C) was attributed to recalcitrant organic matter and/or structural water in clay. The total weight loss of control treatments ranged between 7.3 and 10.0 %. Relative increases observed in C LCa and C HCa with respect to C ($\Delta wt_{measured}$ = 0.50–0.65 % and 2.4–2.7 %, respectively) correlated well the with the mass of applied Ca^{2+} ($\Delta wt_{theoretical}$ = 0.40 % and 2.7 %, respectively). Higher mass losses were observed in the first (30–120 °C) and third (390–750 °C) decomposition stages. This indicated Ca^{2+} application increased the capacity of the soil to retain moisture and interactions with the organic matter/clay fraction.

3.3.3. *Evolution of urea hydrolysis through TG analysis*

The two peaks observed in control samples during the second decomposition stage (120–390°C) merged into a single peak between 210–232°C in U HCa samples (Fig. 4b). The merged peak coincided with the maximum decomposition rate of urea (238.2 ± 1.0 °C, wt. = 69.1 ± 0.4 %, n = 3) (Table S7 and Figure S8). The evolution of urea hydrolysis was observable in U and U LCa treatments (Fig. 4a and c, respectively). The maximum weight loss rate at $T_{peak,urea}$ = 238 °C decreased with increasing reaction time. At t_{end}, no differences with controls indicated all urea had been hydrolysed. The same pattern could be observed for these treatments in GQ and HQ soils (Fig. 4e-f). This indicated T = 238 ºC could be used to monitor and quantify urea hydrolysis.

In line with XRD results, C, C LCa and U HCa showed identical signatures at t_0 and t_{end} (Fig. 4a-c). This evidenced the applied chemical compounds (e.g., nutrient broth, NH_4Cl, urea) produced no changes over time and further confirmed urea hydrolysis was inhibited by U HCa (Fig. 4b). In U and U LCa samples, a new peak was identified between 192–202°C (Fig. 4a and c). This peak was not further observable at tend, in soil samples that received control (Fig. 4a and c) or U HCa (Fig. 4b) treatments, nor the thermal decomposition patterns of the chemicals

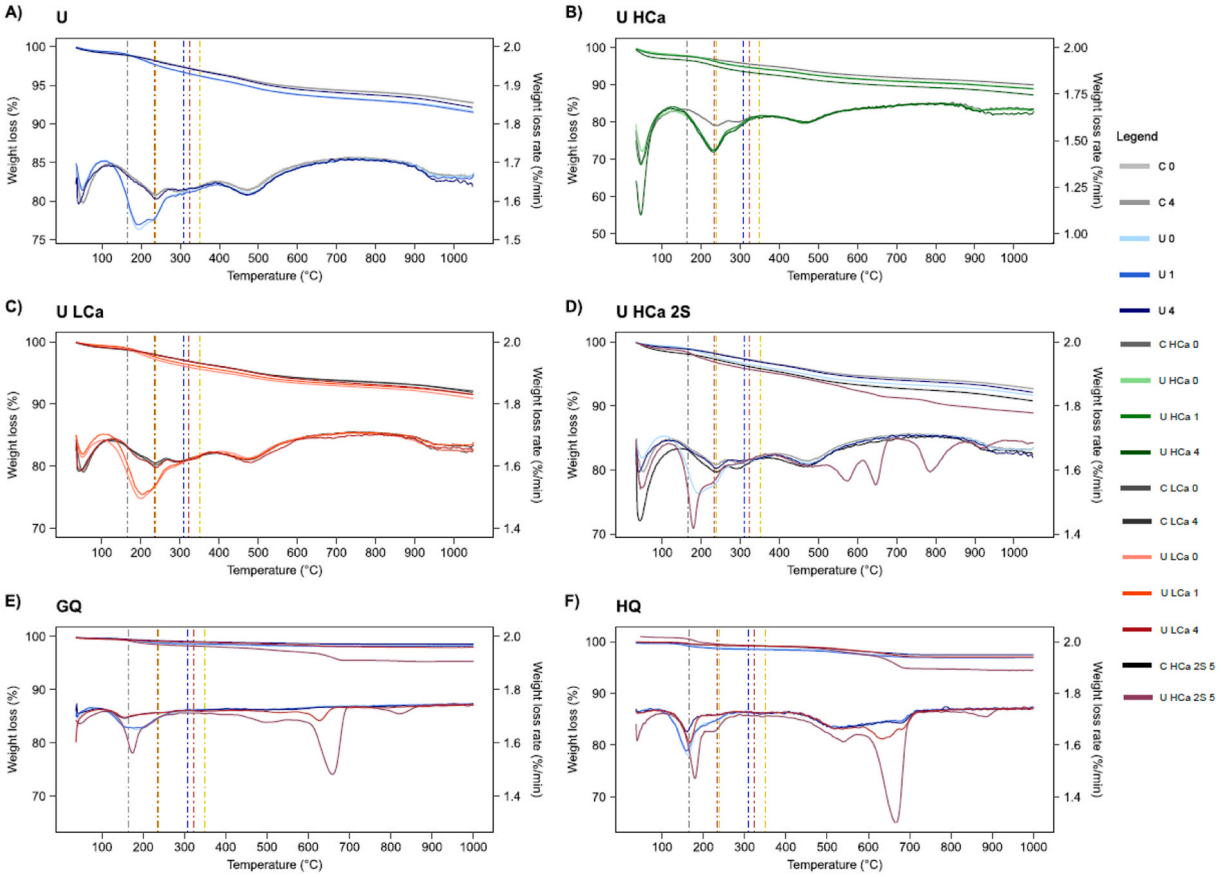

Fig. 4. Thermogravimetric analysis of soil samples throughout biostimulation of MICP: figures a-d) show GLA soil samples that received a specific treatment at various reaction time points; figures e) GQ, and f) HQ, compile several treatments at specific reaction time points. Line colours indicate treatment ID (C, C HCa 2S, C LCa, U, U HCa, U HCa 2S, U LCa) and reaction time ("0", "1", "4", "5" refer to t_r = 1 h, 1, 4 and 5 d, respectively).

that composed treatment solutions (Figure S 8). The peak fell within the main decomposition temperature of $CaCl_2$ (150–200ºC) however, no such peak could be observed in U HCa (Fig. 4b). This indicated it was likely associated with either an intermediate decomposition product or a by-product of urea hydrolysis.

The similar signal of U on day 1 and U HCa 2S on day 5 at T = 238 ºC indicated most urea applied on the second stage of the U HCa 2S treatment on day 4 had not hydrolysed by day 5 (Fig. 4d). Presumably, urea hydrolysis was similarly inhibited by the high calcium dose, as observed with U HCa treatment (Fig. 4b). The inhibition of urea hydrolysis during the second stage could have implications regarding treatment efficiency. On the one hand, it implied the precipitated carbon was produced during the first application. This would reduce the overall carbonation potential since, during treatment solution replacement, dissolved inorganic carbon from the initial urea application would have been partially removed. On the other hand, urea was applied unnecessarily on the second stage. In this regard, one stage treatments, application of calcium solely on the second stage, or applying calcium at doses that allow continuation of urea hydrolysis could improve treatment efficiency. Further research is needed to determine minimum calcium concentrations tolerable by soil indigenous ureolytic bacteria.

3.3.4. *Soil carbonation through TG analysis*

MICP in GLA soil was as evidenced by XRD analysis with U HCa 2S treatment (Fig. 3). U HCa 2S GLA samples decomposed in six main stages: 1) 30–120 °C; 2) 120–372 °C; 3) 372–556 °C; 4) 556–737 °C; 5) 737–900 °C; and 6) 900–1100 °C with total weight loss of 11.4 ± 0.9 % (Fig. 4d). Five new peaks were identified: at 182 ± 2°C during the second decomposition stage; at 575 ± 5 and 651 ± 6 °C during the fourth; 785 ± 4 °C during the fifth; and at 909 ± 4 within the sixth (n = 6, ± is 1sd). The new peaks within decomposition stages 2, 4 and 5 were also detected in GQ and HQ soil samples treated with U HCa 2S and U LCa treatment at t_{end} (Fig. 4e-f). This indicated a relationship with urea hydrolysis and/or MICP. Peaks within 750–900 °C fell within the well documented thermal decomposition range of calcium carbonate [38,51, 68]. The other peaks could be related to other carbonate products. Amorphous calcium carbonate (ACC) loses weight gradually from 550 °C onwards during conversion of $CaCO_3 \bullet H_2O$ to $CaCO_3$ and finally CaO instead of exhibiting the sharp peak of calcite between 750–900ºC [46]. This could explain the observed peaks in GLA soil at 575 and 651 °C with U HCa 2S and between 600–700 °C in GQ and HQ soils with U HCa 2S and U LCa treatments (Fig. 4d-f).

Non-calcium-based carbonates have been reported to decompose at both lower and higher temperatures than calcite. Cerussite ($PbCO_3$) maximum decomposition rate is reported at 189–199 °C [22]. Ammonium carbonate salt (NH_4CO_3) decomposes in one stage with T_{peak} = 140–160 ºC [103]. These could explain the unidentified peaks observed in GLA, GQ and HQ soils with U HCa 2S < 200 °C. Smithsonite ($ZnCO_3$) decomposes in one stage with maximum decomposition rate determined at 265 °C [66]. Rhodochrosite ($MgCO_3$) decomposes in three stages, with peaks at 580, 665 and 900°C [84]. The decomposition peaks of rhodochrosite are similar to the peaks 575, 651 and 909 °C identified in GLA soil (Fig. 4d). Finally, both witherite ($BaCO_3$) and strontianite ($SrCO_3$), have been reported to decompose in two stages, with peaks occurring at 805 and 963 °C [10] and 875 °C and 1010 °C [79], respectively. Unfortunately, we could not evidence presence of these minerals or other carbonate products through XRD analysis.

The calcium carbonate content induced by U HCa 2S treatment in

GLA soil estimated from weight loss within 750–900 ºC was of 3.2 %. Assuming weight losses within 550–750 ºC were related to carbonate products, the total estimated content from TG was 7.2 %. This was in close agreement with the 6.9 % estimated from XRD. Similarly, the estimated calcium carbonate content of GQ and HQ soils treated with U HCa 2S within 550–900 ºC was 4.2 and 7.3 %. This indicated a good agreement with XRD for GQ soil (3.1 %) but an overestimation for HQ soil (4.6 %). The overestimation of TG analysis in HQ soil could be related to overlapping decomposition of carbonate products (>550 ºC) and structural water mass loss of kaolinite, which occurs between 450–700 ºC [80]. The carbonate content induced by the U LCa treatment estimated from the 550–900 ºC region was 0.64 and 0.71 % for GQ and HQ, respectively, coherent with the 0.5 % estimated from XRD analysis.

In summary, XRD and TG analyses evidenced the U HCa 2S treatment maximised calcite precipitation in the three soils studied, U LCa resulted in observable calcite precipitation in GQ and HQ only, while the U treatment did not result in observable carbonate precipitation in any of the tested soils. No definite evidence of carbonate minerals other than calcite could be found, and TG data suggested part of precipitated calcium carbonate could be other carbonation products than calcite.

3.3.5. *ATR-FTIR of GLA soil samples*

ATR-FTIR analysis of GLA soil samples was conducted to investigate further observations of TG analysis (Fig. 5). Absorption bands identified in all samples between 800–1200 and 600–800 cm^{-1} were attributed to quartz, feldspars, and clay minerals, which exhibit a series of overlapping bands within these regions. Bands between 1200 and 900 cm^{-1} (912, 1008, 1032, 1076 and 1163 cm^{-1}) were attributed to asymmetric stretching vibration of the Si-O groups, between 800 and 780 cm^{-1} to symmetric stretching, and 695 cm^{-1} to the symmetric Si-O bending mode [17]. The peak at 668 cm^{-1} indicated the presence of secondary clay minerals [92]. Samples treated with high calcium (C HCa 2S and U HCa) exhibited broad peaks within 1500–1700 (Fig. 5c) and 2700–3700 (Fig. 5d) that were attributed to adsorbed water [56], in line with the higher water mass loss observed for these samples in TG analysis (Fig. 4 and Table S8).

Anhydrous carbonates show four fundamental modes of vibration in ATR spectra, i.e., symmetric stretching (v_1), out-of-plane bending (v_2), asymmetric stretching (v_3) and in-plane bending (v_4). U HCa 2S sample showed the four characteristic modes of vibration of the C-O-C carbonate ion, $v_4 = 712$ cm^{-1}, $v_2 = 875$ cm^{-1} (Fig. 5b), $v_3 = 1412$ cm^{-1}, and $v_1 = 1076$ cm^{-1} (Fig. 5c) [16], confirming the presence of calcium carbonate. ACC is characterised by a shoulder in $v_3 = 1395$–1475 cm^{-1} which is absent in calcium carbonate, the absence of v_2, and the presence of broad bands between 2950 and 3700 cm^{-1} (O-H stretching) and at 1650 cm^{-1} (O-H bending), both corresponding to structural water within ACC [69]. In the U HCa 2S sample, the clear shouldering of the 1412 peak (Fig. 5c) indicated the potential presence of ACC however, the absence of clear O-H absorption bands within 2950 and 3700 cm^{-1} (Fig. 5d) and 1650 cm^{-1} (Fig. 5c) indicated ACC would be anhydrous.

Reflectance spectra of anhydrous carbonates follow trends in band positions with carbonate chemistry, which depend on the mineral structure and the cation size and charge [15]. The v_3 absorption band is the strongest in reflectance spectra and exhibits clear variations with carbonate chemistry, such that the frequency of vibrations increases (wavenumber decreases) with decreasing element radii, with the

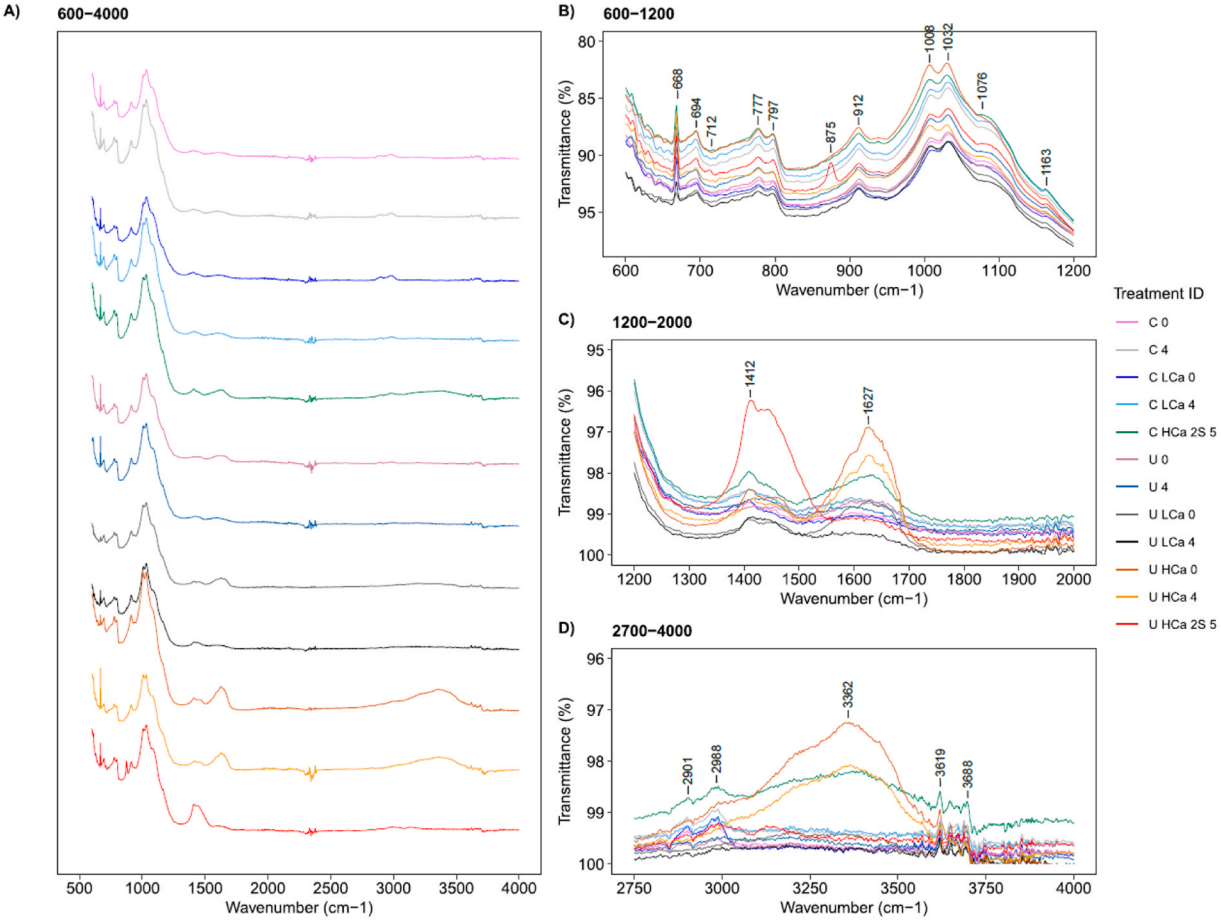

Fig. 5. ATR-FTIR spectra of GLA soil samples following biostimulation of MICP. A) full spectra over wavenumber 600–4000 cm^{-1}; B) 600–1200 cm^{-1}; C) 1200–2000 cm^{-1} and D) 2700–4000 cm^{-1}. Legend indicates treatment ID (C, C HCa 2S, C LCa, U, U HCa, U HCa 2S, U LCa) and reaction time ("0", "4", "5" refer to t_r = 1 h, 4 and 5 d, respectively).

exception of Pb^{2+} [15]. Specifically, strontianite ($SrCO_3$), witherite ($BaCO_3$), cerussite ($PbCO_3$), rhodochrosite ($MnCO_3$) and calcite ($CaCO_3$) show different spectral features and band centres in v_3 within 1402–1495 cm^{-1} [15]. The broad absorption band observed in U HCa 2S sample in the v_3 region (Fig. 5c) thus could be attributed to the overlapping of v_3 absorption bands produced by multiple cations of varying effective radii in the carbonated product. This indicated the peaks identified in the TG analysis could be related to the thermal decomposition of non-calcium carbonates (Fig. 4d). However, the absence of carbonated products other than calcite in XRD (Fig. 3) pointed to their incorporation in calcite. Further research using techniques of higher resolution such as high-resolution X-ray diffraction (HRXRD) are recommended to resolve this as the current methods could not resolve whether ACC or other carbonate products were precipitated.

3.3.6. *SEM-EDS of calcite grains*

SEM-EDS analysis of calcite grains precipitated in GLA soil with the U HCa 2S (t_r = 5 d) revealed calcite was highly porous (Fig. 6a) and contained inclusions of other minerals (Fig. 6f). Porosity was attributed to the encapsulation of bacteria cells, which act as nucleation sites for calcite precipitation [88]. Highly porous calcite has been observed in bioremediation studies of soils [107,23]. Small amounts of Al, Si, S, P, Fe, Mn and Cl (up to 1.2 wt% for Si, under 1 wt% for the other elements) were detected in the EDS analysis from the calcite grains (Fig. 6c-e). However, the signal of these elements was attributed to Al- and Si-rich nano-inclusions of parent soil minerals (Fig. 6b-d) that contain them in higher quantities (Fig. 6f), rather than an incorporation in the calcite lattice. Similar observations have been reported in other studies in which heavy metals were not contained within calcite but were rather attributed to mineral nano inclusions, as observed in Cr-slags [5]. We could not confirm presence of heavy metals, such as Pb in calcite. However, studies in pure cultures have evidenced incorporation of Pb [12] and Zn [9] into MICP, indicating these elements were under the detection limits of EDS technique (<0.1 wt%). In line with TG, XRD and

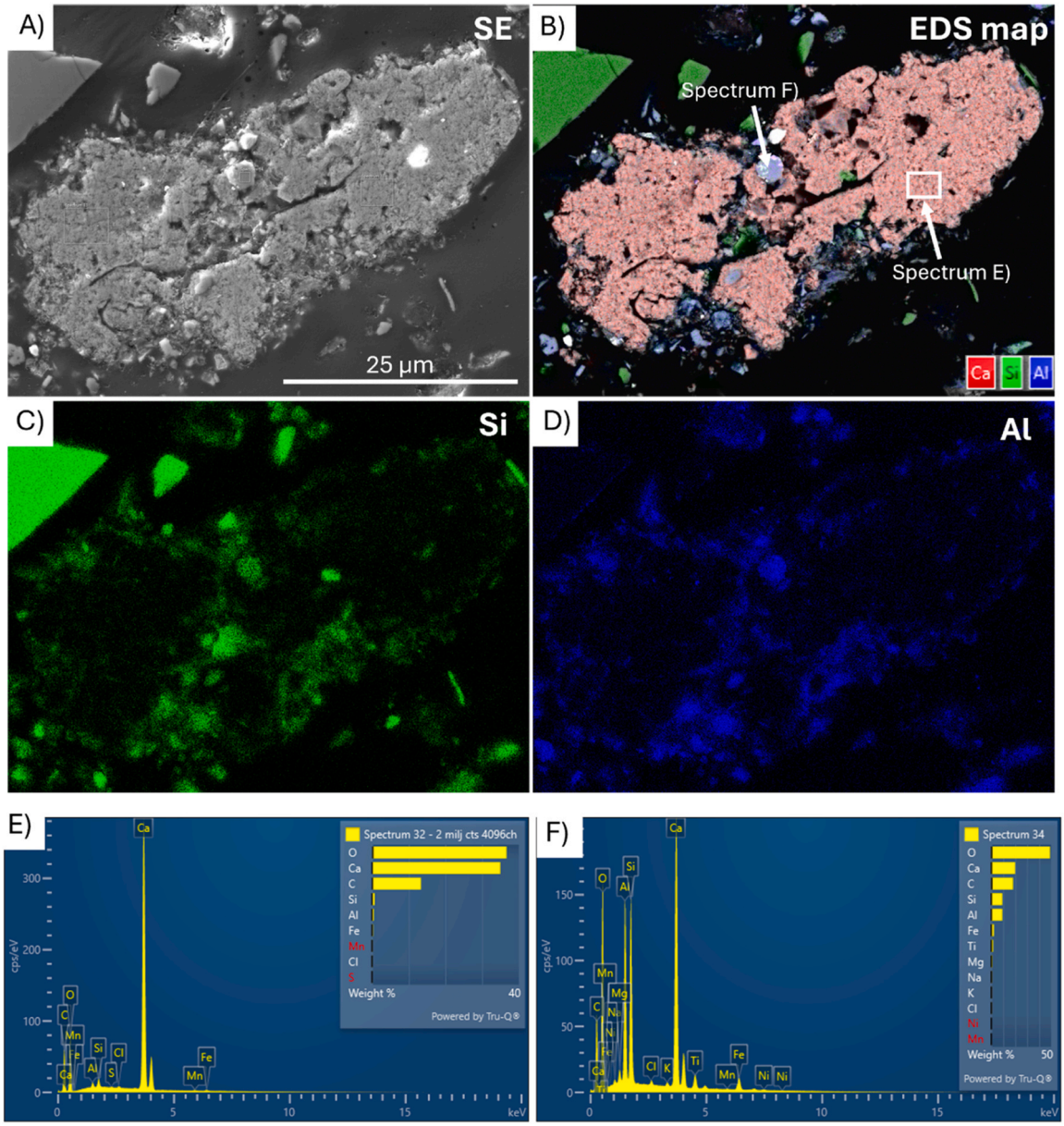

Fig. 6. SEM analysis of precipitated calcite in GLA soil at the end of U HCa 2S treatment. A) secondary electron image showing the porosity within the calcite grain; B) EDS layered elemental map, showing the presence of nano-scale inclusions, rich in Si and Al; C) EDS silicon map; D) EDS aluminium map; E) typical EDS spectrum from calcite grain; F) spectrum from Si- and Al- rich inclusions.

FTIR analysis, no calcite grains were identified in U LCa, U, or control samples.

3.4. Mineralisation of heavy metals

Following confirmation of successful urea hydrolysis and MICP by autochthonous ureolytic bacteria, a sequential extraction on GLA soil was conducted to elucidate distribution of elements across soil fractions, with particular focus on removal from the bioavailable fraction (exchangeable) and immobilisation on the carbonate fraction. Relevant elements in the exchangeable fraction of treated GLA soil samples were Al, Ba, Mn, Pb, Sr and Zn (<2 mM). The other elements measured (As, Cd, Co, Cr, Cu, Mo, Ni, Sb and V) were in trace concentrations (<0.3 mM) throughout treatment (Figure S 7). Importantly, elements present in significant concentration in the total soil fraction (e.g., Cr, V) did not mobilise into the exchangeable fraction as a result of the biogeochemical changes induced urea hydrolysis and/or MICP. Subsequent data analysis thus focused on Al, Ba, Mn, Pb, Sr and Zn.

3.4.1. Elements' behaviour in response to treatment

Element's behaviour in the soil exchangeable (Fig. 7a) and carbonate (Fig. 7b) fractions in response to treatment were analysed through a non-targeted hierarchical cluster analysis (HCA) to elucidate similarities in element behaviour. Samples in the exchangeable fraction were grouped into five clusters, which could be associated to specific environmental conditions induced by treatments (Fig. 7a). Control treatments and early time points ($t_r \leq 1$ d) in which urea hydrolysis might have not been yet significant grouped in two clusters: a) controls with $Ca^{2+} \leq 50$ mM and U samples at t = 1 h (t_0); and b) controls without and with calcium (C, C LCa, C HCa 2S) at t_{end} ($t_r = 4$ or 5 d) plus U LCa samples at $t_r \leq 1$ d. Another cluster was formed by samples treated with U at $t_r > 1$ h indicated a specific effect of urea hydrolysis. Samples that underwent inhibition of urea hydrolysis by U HCa (t_0 to t_{end}) formed another cluster. Finally, samples that underwent urea hydrolysis where calcium was available (U LCa and U HCa 2S treatments at t_{end}) formed a differentiated cluster indicating a specific effect of urea hydrolysis in the presence of Ca^{2+}, potentially related to MICP.

Elements in the exchangeable fraction grouped as Pb-Zn, Sr-Mn and Al-Ba. The Pb-Zn profiles in the exchangeable fraction were nearly identical. The highest Pb-Zn values were observed where urea hydrolysis was insignificant (controls, short reaction time ≤1 d) or inhibited (U HCa). Lower values were observed in samples that underwent urea hydrolysis (U), and the lowest in samples that underwent urea hydrolysis in the presence of calcium (i.e., U LCa and U HCa 2S). For Mn and Sr, instead, higher values were observed in samples that underwent urea hydrolysis (U) and where urea hydrolysis was inhibited by high calcium dose (U HCa). Of the samples that underwent urea hydrolysis, only samples that experienced significant MICP showed low values of Mn and Sr (i.e., U HCa 2S). Al and Ba generally showed higher values in control and urea treatments that excluded calcium at early time points ($t_r = 1$ h).

In the carbonate fraction, elements Ba, Mn, Sr, Pb and Zn formed a cluster whereas Al formed its own cluster (Fig. 7b). The HCA aggregated samples into four groups which reflected a) controls; b) treatments containing urea where urea hydrolysis was insignificant due to short reaction times (U and U LCa, $t_r \leq 1$ d) or inhibition (U HCa); c) samples where urea hydrolysis was significant and either no calcium or low calcium was present (U and U LCa at t_{end}) and d) samples that underwent significant MICP (U HCa 2S at t_{end}). Notably, U HCa 2S induced a marked increase in carbonate bound Pb, Zn, Sr, Ba and Mn compared to other treatments. Samples that underwent urea hydrolysis in absence (U) and presence of low calcium (U LCa) also induced increases of Sr, Ba, Mn and Zn in the carbonate fraction, where presence of calcium resulted in higher increases.

Overall, the HCA evidenced elements in the exchangeable fraction did not respond equally to the applied treatments. Pb and Zn behaviour

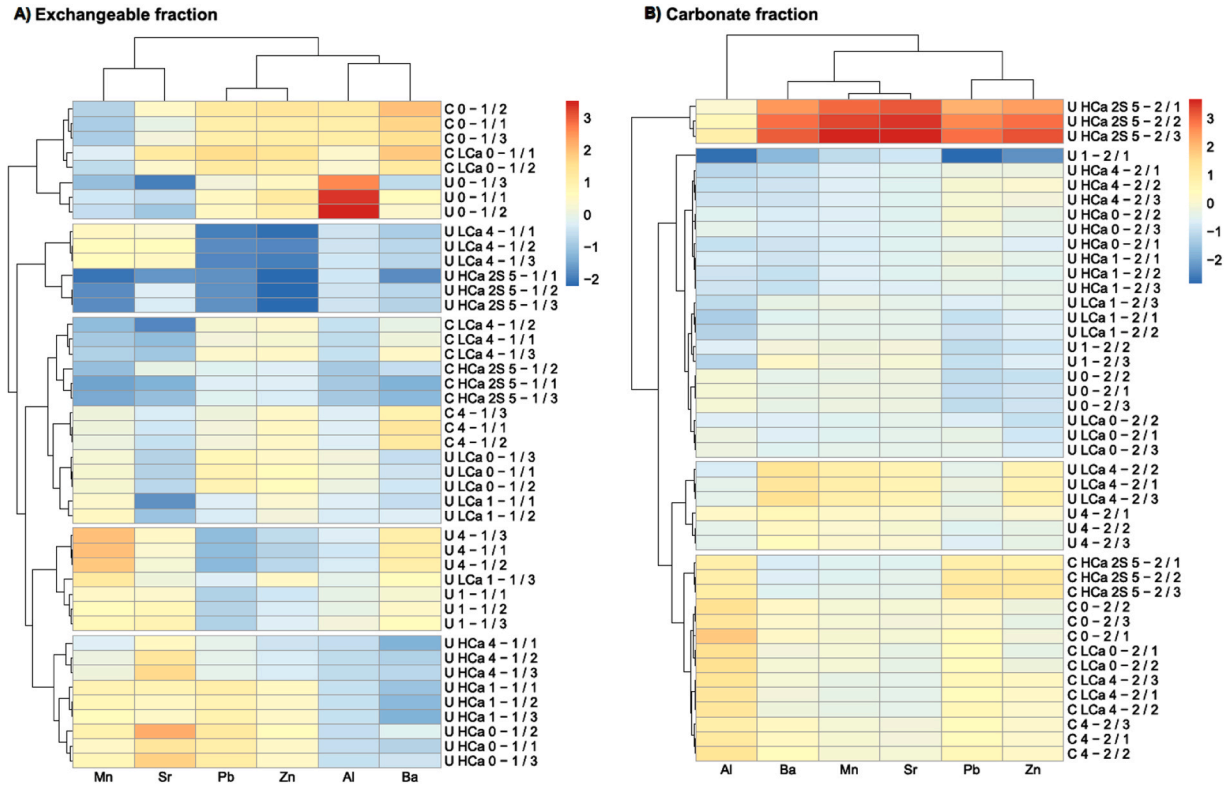

Fig. 7. Euclidean distance heatmap of hierarchical cluster analysis (HCA) of element concentrations determined by ICP-OES on soil exchangeable (A) and carbonate (B) fractions. Sample ID's are organised as: Treatment ID (e.g., "C" for Control), time point (e.g., "4" or 4 days), soil fraction (i.e., 1 = exchangeable, 2 = carbonate) and sample replicate (e.g., /1, replicate 1).

was strongly linked to urea hydrolysis and MICP, indicating potential removal from the exchangeable fraction. This was less evident for Mn, Sr and Ba, whereas Al appeared to behave independently. In the carbonate fraction, the HCA evidenced a much more homogeneous response in elements behaviour to samples that underwent MICP, indicating carbonation of all elements except Al. The sorption tendency of heavy metals varies according to their ionic radii and polarizing ability. Zn and Pb generally exhibit higher sorption tendencies compared to Mn, Sr, and Ba, due to their higher ionic charge density (charge-to-radius ratio). Zn and Pb have a smaller ionic radius and higher polarizing ability, making them more strongly attracted to negatively charged surfaces or ligands. The observed tendency was in agreement with that observed in carbonated soils [47]. Additionally, the HCA indicated a potential mobilisation of Ba, Mn, and Sr into the exchangeable fraction potentially explaining the weaker correlations with urea hydrolysis and MICP compared to Zn and Pb.

3.4.2. *Removal efficiency through soil carbonation*

The element partition from the exchangeable and carbonate fractions of each treatment relative to control (C) at t_0 ($t_r = 1$ h) is presented in Fig. 8. All treatments removed Pb (25–93 %) and Zn (20–98 %) from the exchangeable fraction relative to control (C) at t_0 ($t_r = 1$ h) (Fig. 8a). Pb and Zn removal was significantly higher with urea hydrolysis in absence (U, 71 % Pb and 55 % Zn) and presence of calcium (U LCa and U HCa 2S, 88–93 % Pb and 91–98 % Zn, respectively) compared to controls (25–40 % Pb and 20–46 % Zn). Presence of calcium enhanced removal of Pb and Zn from the exchangeable fraction during urea hydrolysis. This was also observed in bioaugmentation experiments on mine tailings containing Pb and Zn [65].

The highest Pb and Zn partition into the carbonate fraction occurred in samples that underwent significant MICP (U HCa 2S), consistent with observations of bioaugmentation studies on soils and mine tailings [99, 6,41,65]. Interestingly, urea hydrolysis at Ca^{2+} ≤50 mM did not result in significant increases in Pb and Zn in the carbonate fraction (Fig. 8b). For Pb, removal (20–24 %) was observed instead. For Zn, urea hydrolysis (U) did not result in changes in the carbonate fraction and, in presence of 50 mM Ca^{2+}, Zn partition into the carbonate fraction (U LCa, 45 %) was within increases induced by control treatments (19–59 %) (Fig. 8b). The findings for Pb were somewhat surprising. Pb carbonation has been documented both via urea hydrolysis [99] and MICP [99,6]. A significant increase in Pb-oxyhydroxide was determined at t_{end} (U LCa = 0.32 ± 0.02 mM) compared to t_0 (U = 0.25 ± 0.01 mM), which indicated partition of Pb into the oxyhydroxide fraction. Pb solubility is minimum within 8 < pH < 11 in aqueous systems. The stable forms of Pb within 6 < pH < 8.3 comprise cerussite ($PbCO_3$) and hydro-cerussite [$Pb(OH)_2(CO_3)_2$], whilst lead hydroxide [$Pb(OH)_2$] is most stable at

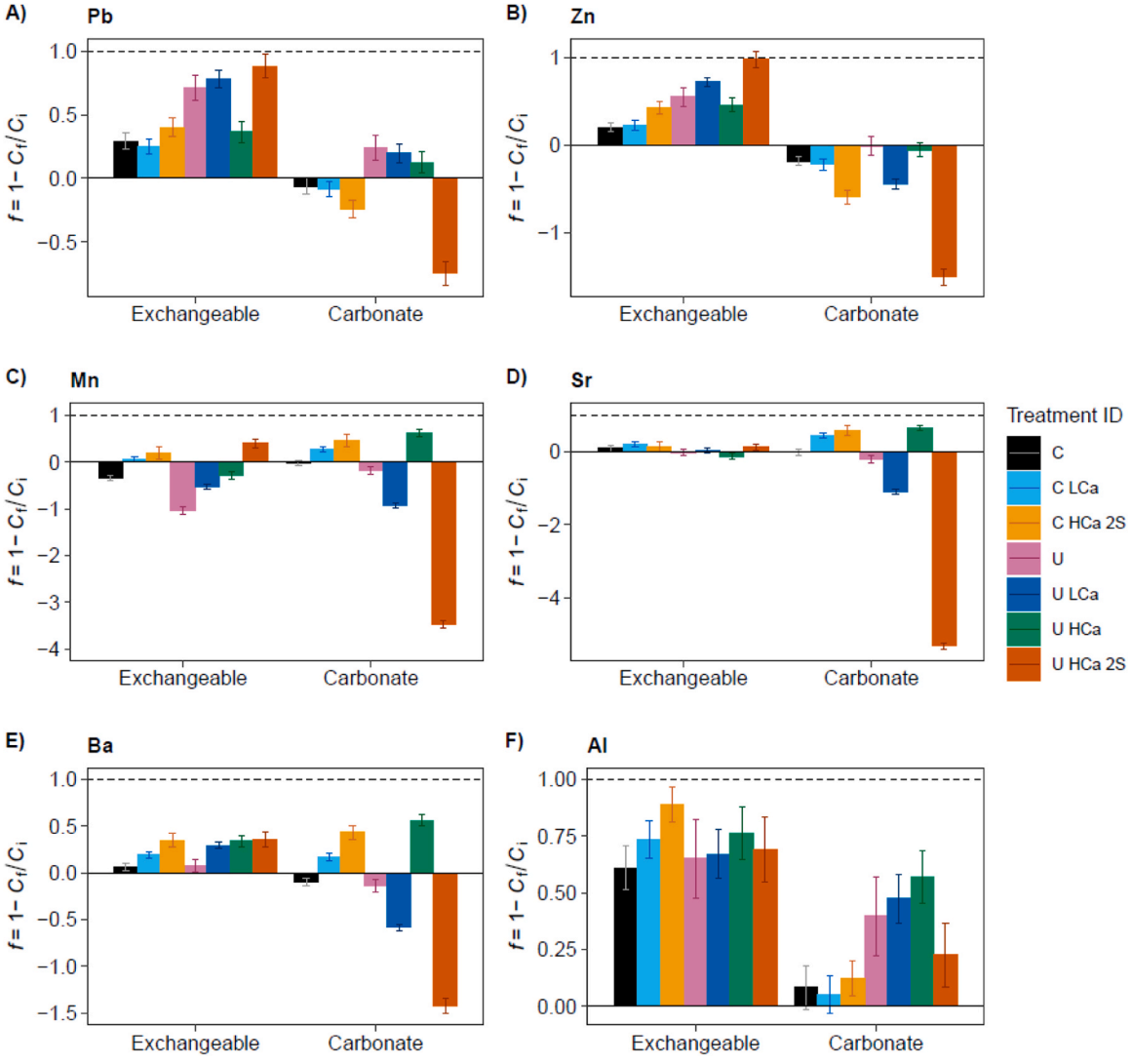

Fig. 8. Normalised element fractionation at t_{end} relative to control (C, t_0) of Pb, Zn, Mn, Ba, Al and Sr in exchangeable and carbonate soil fractions of GLA soil with different treatments. Bars and error bars indicate average and standard error of three replicate samples calculated as indicated in (7).

pH > 8.3 [45]. It was therefore possible that the lower pH induced by MICP (U HCa 2S, pH = 8.4) compared to urea hydrolysis at ≤ 50 mM Ca^{2+} (U and U LCa, pH = 8.8–9) favoured Pb partition into the carbonate fraction rather than the oxyhydroxide fraction and *vice versa*. However, this has not been observed in Pb bioremediation studies [99,6, 41,65] and further investigation is necessary to corroborate it.

Removal of Mn and Sr from the exchangeable fraction only occurred with controls that contained calcium and samples that underwent significant MICP (U HCa 2S) (Fig. 8c-d). Mn removal from the exchangeable was significantly higher with MICP (U HCa 2S, 39 %) compared to controls (5–20 %). Contrary, urea hydrolysis at Ca^{2+} ≤50 mM induced a significant increase in Mn in the exchangeable fraction. The relative increase was smaller in presence of calcium (U LCa, 53 %) than in its absence (U, 103 %). A significant decrease in Mn in the organic matter fraction was determined at t_{end} (U LCa = 1.90 ± 0.03 mM) compared to t_0 (U = 3.0 ± 0.3 mM). This indicated Mn could have mobilised from the organic matter fraction during urea hydrolysis. Mn is a very reactive element which forms complexes with organic matter and is sensitive to changes in redox, pH and microbial activity (for a review see [63]). Mn solubility in alkaline conditions is low, however, reducing conditions such as those that occur in waterlogged soils can trigger dissolution of Mn-organic matter complexes [42]. Additionally, increases in soil solution pH promote soil organic matter dissolution [33]. Reducing conditions could have occurred in this study due to submerged conditions induced by the 1:2 soil-to-solution treatment ratio. Organic matter dissolution could have occurred concomitantly (TC_{GLA} = 3 %) as a result of pH increase from 5 to 9 induced by urea hydrolysis (Fig. 2). Both factors may have resulted in Mn mobilisation into the exchangeable fraction.

Except for the mobilisation from the organic matter fraction, Sr followed the same patterns as Mn. However, changes in Sr were generally small (2–20 %) and not significantly different than controls (Fig. 8d). Samples that underwent significant MICP (U HCa 2S) experienced a large increase in Mn and Sr partition into the carbonate fraction. Urea hydrolysis at Ca^{2+} ≤50 mM also resulted in relative increases, which were higher with calcium (92–109 %) than without (19–20 %). This indicated Mn and Sr partition into the carbonate fraction resulted from urea hydrolysis and increased with increasing calcium content. Similar results for Sr following bioaugmentation of an aquifer sand were reported by Achal et al. [2]. Unfortunately, no studies have been found for Mn. Decreases in the carbonate fraction of both Mn and Sr were recorded in the absence of urea hydrolysis and presence of calcium (28–64 %).

The behaviour of Ba in the exchangeable fraction had similarities with Pb and Zn in that all treatments resulted in removal (6.7–35.0 %) (Fig. 8e). Ba removal was higher in the presence of calcium (C LCa, C HCa 2S, U LCa, U HCa 2S, 19–35 %) than in its absence (C, U, 6.7–7.9 %), independently of its concentration or urea hydrolysis. In the carbonate fraction, Ba showed a similar response to Mn and Sr, in that urea hydrolysis and MICP increased Ba partition into the carbonate fraction, whilst control treatments that contained calcium resulted in removal. Ba could have mobilised from both the organic matter and the oxyhydroxide soil fractions as a result of high calcium application. In the organic matter fraction Ba at t_{end} (U HCa = 0.090 ± 0.003 mM) was significantly lower than at t_0 in absence of calcium (U = 0.15 ± 0.01 mM). Similarly, a significant decrease was determined in the oxyhydroxide fraction at t_{end} (U HCa = 0.11 ± 0.01 mM) compared to t_0 (0.15 ± 0.01 mM). To our knowledge, no studies have been conducted on Ba in the context of MICP.

Similar to Pb, Zn and Ba, all treatments removed Al from the exchangeable fraction (61–89 %) (Fig. 8e). Removal from the carbonate fraction was also recorded (5–57 %), which was larger in samples that contained urea or underwent urea hydrolysis in the absence and presence low calcium (U, U LCa, U HCa, 40–57 %) than controls (5–12 %). In comparison to U, U LCa and U HCa, a lower removal was observed in samples that underwent significant MICP (U HCa 2S, 22 %). Notably, Al was the only element which concentration did not increase in the carbonate fraction with MICP. Divalent cations show more affinity to CO_3^{2-} than trivalent cations and, under standard environmental conditions, Al^{3+} is thought to only be incorporated by coupled substitution with monovalent cations (e.g., dawsonite $NaAl[CO_3](OH)_2$) in hydrous carbonates [13,83]. Furthermore, between pH of 7 and 9, Al precipitates out of solution as gibbsite, $Al(OH)_3$, [18] and may explain the observed changes in Al.

Soils in this study were treated at calcium-to-urea molar ratios selected to investigate different heavy metal immobilisation mechanisms and the potential to maximise heavy metal immobilisation and soil carbonation. Overall, the results of the sequential extraction evidenced MICP maximised partition of Pb, Zn, Mn, Sr, Ba into the carbonate fraction, evidencing the mechanism of element immobilisation was through calcium carbonate precipitation. At a lower calcium-to-urea ratio, however, Zn, Mn, Sr and Ba partition into the carbonate fraction decreased, indicating their degree or carbonation was dependant on calcite precipitation. Through urea hydrolysis, partition of Mn, Sr and Ba into the carbonate fraction indicated their immobilisation as carbonates occurred to some extent. Instead, Pb partition into the oxyhydroxide fraction could have occurred when urea hydrolysis was significant but calcium carbonate precipitation was insignificant. This alternative immobilisation mechanism could be favoured by the higher pH induced by urea hydrolysis due to the greater affinity of Pb for OH^- instead of CO_3^{2-} at pH > 8.3 [45]. To corroborate the mobilisation and immobilisation mechanisms during urea hydrolysis and MICP, the behaviour of these elements in soil fractions other than exchangeable and carbonate should be investigated in further detail. In this study we only conducted the full sequential extraction on U, U LCa and U HCa, limiting our interpretation. We recommend further research focus on the potential precipitation of toxic elements as oxyhydroxides versus carbonates. Partition of toxic elements into the oxyhydroxide fraction could be a more labile pool for element immobilisation compared to carbonation and have implications for their long-term bioremediation stability. The results of the sequential extraction would have been greatly complemented from a more detailed analysis on the soil-solution chemical composition during treatment. In particular, the dissolution of organic matter during urea hydrolysis could corroborate observations made for Mn and Ba.

For the most efficient two-stage treatment, we observed both a reduction in the exchangeable fraction compared to the control and an increase in the carbonate fraction. However, some of this reduction may not be attributed solely to immobilisation in the carbonate fraction but rather to metal loss during solution replacement. Additionally, solution replacement likely removed dissolved CO_2, limiting carbonation and, consequently, reducing element immobilisation. Since the stability of immobilised toxic elements depends on the extent of carbonation, this could affect their long-term resistance to environmental stressors. MICP is particularly sensitive to conditions such as wet-dry cycles, freeze-thaw cycles, and acid rain, but greater carbonation can enhance stability and improve resilience to these effects [64]. Therefore, optimising this treatment to maximise soil carbonation would not only improve bioremediation efficiency but also reinforce the durability of immobilised contaminants, ensuring greater long-term stability under variable environmental conditions.

Powder XRD did not resolve precipitated mineral phases other than calcite and SEM-EDS of calcite grains could not confirm incorporation of elements into MICP. FTIR-ATR could not discern between heavy metal carbonates, ACC and incorporation of metals into calcite due to overlapping of absorption bands around v_3. Higher resolution techniques may be necessary in complex soil environmental samples with moderate toxic element concentrations such as in this study.

Finally, the reproducibility of pH, NH_4^+, XRD and TG patterns observed across different soils herein indicated our findings are generalisable across soils of different physicochemical and microbiological compositions. However, our data also evidenced variability across soils particularly on absolute numbers such as precipitated carbonate

content. It is well established that soil physicochemical properties influence microbial activity and ultimately MICP. In addition, differing levels of pollution and chemical mixtures add further complexity to the assessment of the potential of MICP as a bioremediation technique. Future research on soils with differing microbial compositions, soil physicochemical properties and toxicity levels are encouraged to elucidate the relevance and interaction of different parameters, and how these affect the bioremediation efficiency via biostimulation of MICP.

4. Conclusions

This study investigated the simultaneous bioremediation of heavy metals through biostimulation of MICP at varying calcium-to-urea ratios. The comparable urea hydrolysis and MICP observed in an urban soil containing 5–7 times Pb, Zn, Mn, Sr, Ba and Al compared to two regional uncontaminated soils indicated robustness of autochthonous ureolytic bacteria against moderate levels of pollution. Bacterial activity, soil carbonation and element immobilisation mechanisms were influenced by the calcium-to-urea molar ratio. Bacterial activity was negatively affected by increasing initial calcium application across soils independently of toxic element concentration. Delayed urea hydrolysis to inhibition was attributed to early encapsulation of bacterial cells by MICP, resulting in low to insignificant soil carbonation. Introducing calcium once urea hydrolysis was significant maximised element immobilization and carbon sequestration through mineral trapping. Through this approach, equimolar calcium-to-urea of 333 mM maximised soil carbonation, removal of Pb and Zn from the exchangeable fraction, and Pb, Zn, Mn, Ba, Sr, and Ba carbonation. The results of this study evidence soils containing moderate levels of heavy metals could be bioremediated through biostimulation of MICP, potentially decreasing treatment costs due to ubiquitousness of autochthonous bacteria. The use of non-targeted multivariate analysis was useful in revealing similar patterns across elements and we recommend their incorporation as a data analysis technique in future studies on complex soil systems. Maximising soil carbonation is recommended to enhance element immobilisation through carbonation and stability against environmental conditions such as acid rain, whist enhancing additional ecosystem services such as permanent carbon sequestration and storage and enhancement of soil mechanical properties.

Environmental implication

The results of this study highlight the potential of soil's autochthonous ureolytic bacteria from vacant and derelict land for the bioremediation of heavy metals through Microbial-Induced Calcite Precipitation. Furthermore, it establishes a precedence of multiple element immobilisation and differing immobilisation mechanisms which were element and treatment dependant. Based on the presented results, we recommend a two-step treatment with equimolar urea-to-calcium ratio of 333 mM to maximise carbon sequestration and element partition into the carbonate fraction in the context of bioremediation via MICP.

Funding sources

GALLANT is funded by the Natural Environment Research Council as part of the Changing the Environment Programme [grant number NE/W005042/1].

CRediT authorship contribution statement

Khaksar Najafi Elmira: Writing – review & editing. **MacDonald John:** Writing – review & editing, Funding acquisition, Conceptualization. **Bass Adrian M.:** Writing – review & editing, Funding acquisition, Conceptualization. **Unluer Cise:** Writing – review & editing, Supervision, Project administration, Funding acquisition, Conceptualization. **Comadran Casas Carla:** Writing – original draft, Resources, Methodology, Investigation, Formal analysis, Data curation, Conceptualization. **Gauchotte-Lindsay Caroline:** Writing – review & editing, Resources, Project administration, Methodology, Funding acquisition, Formal analysis, Conceptualization. **Spruzeniece Liene:** Writing – review & editing, Methodology, Formal analysis.

Declaration of Competing Interest

The authors declare the following financial interests/personal relationships which may be considered as potential competing interests: Carla Comadran Casas reports financial support was provided by UK Research and Innovation Natural Environment Research Council. If there are other authors, they declare that they have no known competing financial interests or personal relationships that could have appeared to influence the work reported in this paper.

Acknowledgements

Special thanks are given to the funding body UKRI Natural Environment Research Council, to A. Hunter, E. Palmer, Dr C. Brolly, Dr C. Wilson, K. Roberts and Dr M. Wildman of the University of Glasgow for their technical support, to the Geoanalytical Electron Microscopy and Spectroscopy (GEMS) facility at the University of Glasgow for the support and assistance with electron microscopy, to Dr V. Olive and Dr G. MacKinnon of the Scottish Universities Environmental Research Centre (SUERC), to E. Murray of the GALLANT research project for the administrative support, to J. King of Hugh King Tillicoultry Quarries for sourcing material, and to J. Duckett of the Glasgow City Council for the technical assistance.

Appendix A. Supporting information

Supplementary data associated with this article can be found in the online version at doi:10.1016/j.jhazmat.2025.137691.

Data availability

Data will be made available on request.

References

[1] Achal, V., Pan, X., Zhang, D., 2011. Remediation of copper-contaminated soil by Kocuria flava CR1, based on microbially induced calcite precipitation. Ecol Eng 37 (10), 1601–1605. https://doi.org/10.1016/j.ecoleng.2011.06.008.
[2] Achal, V., Pan, X., Zhang, D., 2012. Bioremediation of strontium (Sr) contaminated aquifer quartz sand based on carbonate precipitation induced by Sr resistant Halomonas sp. Chemosphere 89 (6), 764–768. https://doi.org/10.1016/j.chemosphere.2012.06.064.
[3] Achal, V., Pan, X., Fu, Q., Zhang, D., 2012. Biomineralization based remediation of As (III) contaminated soil by Sporosarcina ginsengisoli. J Hazard Mater 201, 178–184. https://doi.org/10.1016/j.jhazmat.2011.11.067.
[4] Achal, V., Pan, X., 2014. Influence of calcium sources on microbially induced calcium carbonate precipitation by Bacillus sp. CR2. Appl Biochem Biotechnol 173, 307–317. https://doi.org/10.1007/s12010-014-0842-1.
[5] Achal, V., Pan, X., Lee, D.J., Kumari, D., Zhang, D., 2013. Remediation of Cr (VI) from chromium slag by biocementation. Chemosphere 93 (7), 1352–1358. https://doi.org/10.1016/j.chemosphere.2013.08.008.
[6] Achal, V., Pan, X., Zhang, D., Fu, Q., 2012. Bioremediation of Pb-contaminated soil based on microbially induced calcite precipitation. J Microbiol Biotechnol 22 (2), 244–247. https://doi.org/10.4014/jmb.1108.08033.
[7] Al Qabany, A., Soga, K., 2014. Effect of chemical treatment used in MICP on engineering properties of cemented soils. In Bio-and chemo-mechanical processes in geotechnical engineering: géotechnique symposium in print 2013. ICE Publishing, pp. 107–115. https://doi.org/10.1680/bcmpge.60531.010.
[8] Al Qabany, A., Soga, K., Santamarina, C., 2012. Factors affecting efficiency of microbially induced calcite precipitation. J Geotech Geoenviron Eng 138 (8), 992–1001. https://doi.org/10.1061/(ASCE)GT.1943-5606.0000666.
[9] Ali, A., Li, M., Su, J., Li, Y., Wang, Z., Bai, Y., Ali, E.F., Shaheen, S.M., 2022. Brevundimonas diminuta isolated from mines polluted soil immobilized cadmium (Cd2+) and zinc (Zn2+) through calcium carbonate precipitation: microscopic and spectroscopic investigations. Sci Total Environ 813, 152668. https://doi.org/10.1016/j.scitotenv.2021.152668.

[10] Arvanitidis, I., Siche, D., Seetharaman, S., 1996. A study of the thermal decomposition of BaCO3. Metall Mater Trans B 27, 409–416. https://doi.org/10.1007/BF02914905.
[11] Bache, B.W., 1984. The role of calcium in buffering soils. Plant, Cell Environ 7 (6), 391–395. https://doi.org/10.1111/j.1365-3040.1984.tb01428.x.
[12] Bai, H., Liu, D., Zheng, W., Ma, L., Yang, S., Cao, J., Lu, X., Wang, H., Mehta, N., 2021. Microbially-induced calcium carbonate precipitation by a halophilic ureolytic bacterium and its potential for remediation of heavy metal-contaminated saline environments. Int Biodeterior Biodegrad 165, 105311. https://doi.org/10.1016/j.ibiod.2021.105311.
[13] Bayarjargal, L., Spahr, D., Milman, V., Marquardt, J., Giordano, N., Winkler, B., 2023. Anhydrous aluminum carbonates and isostructural compounds. Inorg Chem 62 (34), 13910–13918.
[14] Bhattacharya, A., Naik, S.N., Khare, S.K., 2018. Harnessing the bio-mineralization ability of urease producing serratia marcescens and enterobacter cloacae EMB19 for remediation of heavy metal cadmium (II). J Environ Manag 215, 143–152. https://doi.org/10.1016/j.jenvman.2018.03.055.
[15] Bishop, J.L., King, S.J., Lane, M.D., Brown, A.J., Lafuente, B., Hiroi, T., Roberts, R., Swayze, G.A., Lin, J.F., Sánchez Román, M., 2021. Spectral properties of anhydrous carbonates and nitrates. e2021EA001844 Earth Space Sci 8 (10). https://doi.org/10.1029/2021EA001844.
[16] Bosch-Reig, F., Adelantado, J.G., Moreno, M.M., 2002. FTIR quantitative analysis of calcium carbonate (calcite) and silica (quartz) mixtures using the constant ratio method. Application to geological samples. Talanta 58 (4), 811–821. https://doi.org/10.1016/S0039-9140(02)00372-7.
[17] Bosch-Reig, F., Gimeno-Adelantado, J.V., Bosch-Mossi, F., Doménech-Carbó, A., 2017. Quantification of minerals from ATR-FTIR spectra with spectral interferences using the MRC method. Spectrochim Acta Part A: Mol Biomol Spectrosc 181, 7–12. https://doi.org/10.1016/j.saa.2017.02.012.
[18] Brautigan, D.J., Rengasamy, P., Chittleborough, D.J., 2012. Aluminium speciation and phytotoxicity in alkaline soils. Plant Soil 360, 187–196. https://doi.org/10.1007/s11104-012-1232-5.
[19] Burbank, M.B., Weaver, T.J., Williams, B.C., Crawford, R.L., 2012. Urease activity of ureolytic bacteria isolated from six soils in which calcite was precipitated by indigenous bacteria. Geomicrobiol J 29 (4), 389–395. https://doi.org/10.1080/01490451.2011.575913.
[20] Cardoso, R., Borges, I., Vieira, J., Duarte, S.O., Monteiro, G.A., 2023. Interactions between clay minerals, bacteria growth and urease activity on biocementation of soils. Appl Clay Sci 240, 106972. https://doi.org/10.1016/j.clay.2023.106972.
[21] Chai, L., Huang, S., Yang, Z., Peng, B., Huang, Y., Chen, Y., 2009. Cr (VI) remediation by indigenous bacteria in soils contaminated by chromium-containing slag. J Hazard Mater 167 (1-3), 516–522. https://doi.org/10.1016/j.jhazmat.2009.01.030.
[22] Chapter 12 Decomposition of carbonates, 1999. Galwey, A.K., Brown, M.E. (ed) Studies in Physical and Theoretical Chemistry, pp. 345-364. https://doi.org/10.1016/S0167-6881(99)80014-7.
[23] Chen, X., Achal, V., 2019. Biostimulation of carbonate precipitation process in soil for copper immobilization. J Hazard Mater 368, 705–713. https://doi.org/10.1016/j.jhazmat.2019.01.108.
[24] Chung, H., Kim, S.H., Nam, K., 2020. Inhibition of urea hydrolysis by free Cu concentration of soil solution in microbially induced calcium carbonate precipitation. Sci Total Environ 740, 140194. https://doi.org/10.1016/j.scitotenv.2020.140194.
[25] Clarà Saracho, A., Marek, E.J., 2024. Uncovering the dynamics of urease and carbonic anhydrase genes in ureolysis, carbon dioxide hydration, and calcium carbonate precipitation. Environmental Science & Technology 58 (2), 1199–1210. https://doi.org/10.1021/acs.est.3c06617.
[26] Comadran-Casas, C., Brüggemann, N., Jorat, M.E., 2024. Greenhouse gas fluxes of microbial-induced calcite precipitation at varying urea-to-calcium concentrations. Eur J Soil Sci 75 (3), e13516. https://doi.org/10.1111/ejss.13516.
[27] Cui, M.J., Teng, A., Chu, J., Cao, B., 2022. A quantitative, high-throughput urease activity assay for comparison and rapid screening of ureolytic bacteria. Environ Res 208, 112738. https://doi.org/10.1016/j.envres.2022.112738.
[28] de Mendiburu, F., 2021. _agricolae: statistical procedures for agricultural research_. R Package Version 1, 3–5. ⟨https://CRAN.R-project.org/package=agricolae⟩.
[29] DeJong, J.T., Fritzges, M.B., Nüsslein, K., 2006. Microbially induced cementation to control sand response to undrained shear. J Geotech Geoenviron Eng 132 (11), 1381–1392. https://doi.org/10.1061/(ASCE)1090-0241(2006)132:11(1381).
[30] Diamond, S., Kinter, E.B., 1966. Adsorption of calcium hydroxide by montmorillonite and kaolinite. J Colloid Interface Sci 22 (3), 240–249. https://doi.org/10.1016/0021-9797(66)90029-4.
[31] Do, H., Wang, Y., Long, Z., Ketehouli, T., Li, X., Zhao, Z., Li, M., 2020. A psychrotolerant Ni-resistant Bacillus cereus D2 induces carbonate precipitation of nickel at low temperature. Ecotoxicol Environ Saf 198, 110672. https://doi.org/10.1016/j.ecoenv.2020.110672.
[32] Dupraz, S., Parmentier, M., Ménez, B., Guyot, F., 2009. Experimental and numerical modeling of bacterially induced pH increase and calcite precipitation in saline aquifers. Chem Geol 265 (1–2), 44–53. https://doi.org/10.1016/j.chemgeo.2009.05.003.
[33] Evans, C.D., Jones, T.G., Burden, A., Ostle, N., Zieliński, P., Cooper, M.D., Peacock, M., Clark, J.M., Oulehle, F., Cooper, D., Freeman, C., 2012. Acidity controls on dissolved organic carbon mobility in organic soils. Glob Change Biol 18 (11), 3317–3331. https://doi.org/10.1111/j.1365-2486.2012.02794.x.
[34] Fang, L., Niu, Q., Cheng, L., Jiang, J., Yu, Y.Y., Chu, J., Achal, V., You, T., 2021. Ca-mediated alleviation of Cd2+ induced toxicity and improved Cd2+ biomineralization by Sporosarcina pasteurii. Sci Total Environ 787, 147627. https://doi.org/10.1016/j.scitotenv.2021.147627.
[35] Fu, T., Saracho, A.C., Haigh, S.K., 2023. Microbially induced carbonate precipitation (MICP) for soil strengthening: A comprehensive review. Biogeotechnics, 100002. https://doi.org/10.1016/j.bgtech.2023.100002.
[36] Fujita, Y., Ferris, F.G., Lawson, R.D., Colwell, F.S., Smith, R.W., 2000. Subscribed content calcium carbonate precipitation by ureolytic subsurface bacteria. Geomicrobiol J 17 (4), 305–318. https://doi.org/10.1080/782198884.
[37] Fujita, Y., Redden, G.D., Ingram, J.C., Cortez, M.M., Ferris, F.G., Smith, R.W., 2004. Strontium incorporation into calcite generated by bacterial ureolysis. Geochim Et Cosmochim Acta 68 (15), 3261–3270. https://doi.org/10.1016/j.gca.2003.12.018.
[38] Galan, I., Glasser, F.P., Andrade, C., 2013. Calcium carbonate decomposition. J Therm Anal Calorim 111, 1197–1202. https://doi.org/10.1007/s10973-012-2290-x.
[39] Gat, D., Ronen, Z., Tsesarsky, M., 2017. Long-term sustainability of microbial-induced CaCO3 precipitation in aqueous media. Chemosphere 184, 524–531. https://doi.org/10.1016/j.chemosphere.2017.06.015.
[40] Gianfreda, L., Rao, M.A., Violante, A., 1992. Adsorption, activity and kinetic properties of urease on montmorillonite, aluminium hydroxide and AL (OH) x-montmorillonite complexes. Soil Biol Biochem 24 (1), 51–58. https://doi.org/10.1016/0038-0717(92)90241-O.
[41] Govarthanan, M., Lee, K.J., Cho, M., Kim, J.S., Kamala-Kannan, S., Oh, B.T., 2013. Significance of autochthonous Bacillus sp. KK1 on biomineralization of lead in mine tailings. Chemosphere 90 (8), 2267–2272. https://doi.org/10.1016/j.chemosphere.2012.10.038.
[42] Grybos, M., Davranche, M., Gruau, G., Petitjean, P., Pédrot, M., 2009. Increasing pH drives organic matter solubilization from wetland soils under reducing conditions. Geoderma 154 (1-2), 13–19. https://doi.org/10.1016/j.geoderma.2009.09.001.
[43] Haynes, W.M. (Ed.), 2015. CRC Handbook of Chemistry and Physics, 95th Edition. CRC Press LLC, Boca Raton: FL, pp. 4–46. https://doi.org/10.1201/9781315380476. 2014.
[44] He, J., Chen, X., Zhang, Q., Achal, V., 2019. More effective immobilization of divalent lead than hexavalent chromium through carbonate mineralization by Staphylococcus epidermidis HJ2. Int Biodeterior Biodegrad 140, 67–71. https://doi.org/10.1016/j.ibiod.2019.03.012.
[45] Hem, J.D., Durum, W.H., 1973. Solubility and occurrence of lead in surface water. J (Am Water Works Assoc 562–568. ⟨https://www.jstor.org/stable/41267396⟩.
[46] Ihli, J., Wong, W.C., Noel, E.H., Kim, Y.Y., Kulak, A.N., Christenson, H.K., Duer, M.J., Meldrum, F.C., 2014. Dehydration and crystallization of amorphous calcium carbonate in solution and in air. Nat Commun 5 (1), 3169. https://doi.org/10.1038/ncomms4169.
[47] Jalali, M., Moradi, F., 2013. Competitive sorption of Cd, Cu, Mn, Ni, Pb and Zn in polluted and unpolluted calcareous soils. Environ Monit Assess 185, 8831–8846. https://doi.org/10.1007/s10661-013-3216-1.
[48] Jiang, N.J., Liu, R., Du, Y.J., Bi, Y.Z., 2019. Microbial induced carbonate precipitation for immobilizing Pb contaminants: Toxic effects on bacterial activity and immobilization efficiency. Sci Total Environ 672, 722–731. https://doi.org/10.1016/j.scitotenv.2019.03.294.
[49] Kang, C.H., Han, S.H., Shin, Y., Oh, S.J., So, J.S., 2014. Bioremediation of Cd by microbially induced calcite precipitation. Appl Biochem Biotechnol 172, 2907–2915. https://doi.org/10.1007/s12010-014-0737-1.
[50] Kang, C.H., Oh, S.J., Shin, Y., Han, S.H., Nam, I.H., So, J.S., 2015. Bioremediation of lead by ureolytic bacteria isolated from soil at abandoned metal mines in South Korea. Ecol Eng 74, 402–407. https://doi.org/10.1016/j.ecoleng.2014.10.009.
[51] Karunadasa, K.S., Manoratne, C.H., Pitawala, H.M.T.G.A., Rajapakse, R.M.G., 2019. Thermal decomposition of calcium carbonate (calcite polymorph) as examined by in-situ high-temperature X-ray powder diffraction. J Phys Chem Solids 134, 21–28. https://doi.org/10.1016/j.jpcs.2019.05.023.
[52] Khonje, D.J., Varsa, E.C., Klubek, B., 1989. The acidulation effects of nitrogenous fertilizers on selected chemical and microbiological properties of soil. Commun Soil Sci Plant Anal 20 (13-14), 1377–1395. https://doi.org/10.1080/00103628909368156.
[53] Kim, Y., Kwon, S., Roh, Y., 2021. Effect of divalent cations (Cu, Zn, Pb, Cd, and Sr) on microbially induced calcium carbonate precipitation and mineralogical properties. Front Microbiol 12, 646748. https://doi.org/10.3389/fmicb.2021.646748.
[54] Kissel, D.E., Sonon, L., Vendrell, P.F., Isaac, R.A., 2009. Salt concentration and measurement of soil pH. Commun Soil Sci Plant Anal 40 (1-6), 179–187. https://doi.org/10.1080/00103620802625377.
[55] Krajewska, B., 2009. Ureases I. Functional, catalytic and kinetic properties: a review. J Mol Catal B: Enzym 59 (1-3), 9–21. https://doi.org/10.1016/j.molcatb.2009.01.003.
[56] Krivoshein, P.K., Volkov, D.S., Rogova, O.B., Proskurnin, M.A., 2022. FTIR photoacoustic and ATR spectroscopies of soils with aggregate size fractionation by dry sieving. ACS Omega 7 (2), 2177–2197. https://doi.org/10.1021/acsomega.1c05702.
[57] Ku, H.H., 1966. Notes on the use of propagation of error formulas. J Res Natl Bur Stand 70 (4), 263.
[58] Kumari, D., Li, M., Pan, X., Xin-Yi, Q., 2014. Effect of bacterial treatment on Cr (VI) remediation from soil and subsequent plantation of Pisum sativum. Ecol Eng 73, 404–408. https://doi.org/10.1016/j.ecoleng.2014.09.093.

[59] Kumari, D., Pan, X., Lee, D.J., Achal, V., 2014. Immobilization of cadmium in soil by microbially induced carbonate precipitation with Exiguobacterium undae at low temperature. Int Biodeterior Biodegrad 94, 98–102. https://doi.org/10.1016/j.ibiod.2014.07.007.
[60] Li, M., Cheng, X., Guo, H., 2013. Heavy metal removal by biomineralization of urease producing bacteria isolated from soil. Int Biodeterior Biodegrad 76, 81–85. https://doi.org/10.1016/j.ibiod.2012.06.016.
[61] Li, M., Cheng, X., Guo, H., Yang, Z., 2016. Biomineralization of carbonate by terrabacter tumescens for heavy metal removal and biogrouting applications. J Environ Eng 142 (9), C4015005. https://doi.org/10.1061/(ASCE)EE.1943-7870.0000970.
[62] Li, L., Mao, K., Ippolito, J.A., Xing, W., Chen, X., Zhu, W., Cheng, Y., 2022. Calcium amendments affect heavy metal bioavailability in acidic and calcareous soils. Int J Environ Sci Technol (10), 1. https://doi.org/10.1007/s13762-021-03840-y.
[63] Li, H., Santos, F., Butler, K., Herndon, E., 2021. A critical review on the multiple roles of manganese in stabilizing and destabilizing soil organic matter. Environ Sci Technol 55 (18), 12136–12152. https://doi.org/10.1021/acs.est.1c00299.
[64] Liu, S., Wen, K., Armwood, C., Bu, C., Li, C., Amini, F., Li, L., 2019. Enhancement of MICP-treated sandy soils against environmental deterioration. J Mater Civ Eng 31 (12), 04019294. https://doi.org/10.1061/(ASCE)MT.1943-5533.0002959.
[65] Liu, P., Zhang, Y., Tang, Q., Shi, S., 2021. Bioremediation of metal-contaminated soils by microbially-induced carbonate precipitation and its effects on ecotoxicity and long-term stability. Biochem Eng J 166, 107856. https://doi.org/10.1016/j.bej.2020.107856.
[66] Liu, Y., Zhao, J., Zhang, H., Zhu, Y., Wang, Z., 2004. Thermal decomposition of basic zinc carbonate in nitrogen atmosphere. Thermochim Acta 414 (2), 121–123. https://doi.org/10.1016/j.tca.2003.12.004.
[67] Lyu, C., Qin, Y., Chen, T., Zhao, Z., Liu, X., 2022. Microbial induced carbonate precipitation contributes to the fates of Cd and Se in Cd-contaminated seleniferous soils. J Hazard Mater 423, 126977. https://doi.org/10.1016/j.jhazmat.2021.126977.
[68] Manning, D.A.C., Lopez-Capel, E., Barker, S., 2005. Seeing soil carbon: use of thermal analysis in the characterization of soil C reservoirs of differing stability. Mineral Mag 69 (4), 425–435. https://doi.org/10.1180/0026461056940260.
[69] Mehta, N., Gaëtan, J., Giura, P., Azaïs, T., Benzerara, K., 2022. Detection of biogenic amorphous calcium carbonate (ACC) formed by bacteria using FTIR spectroscopy. Spectrochim Acta Part A: Mol Biomol Spectrosc 278, 121262. https://doi.org/10.1016/j.saa.2022.121262.
[70] Millo, C., Dupraz, S., Ader, M., Guyot, F., Thaler, C., Foy, E., Ménez, B., 2012. Carbon isotope fractionation during calcium carbonate precipitation induced by ureolytic bacteria. Geochim Et Cosmochim Acta 98, 107–124. https://doi.org/10.1016/j.gca.2012.08.029.
[71] Mitchell, J.K., Santamarina, J.C., 2005. Biological considerations in geotechnical engineering. J Geotech Geoenviron Eng 131 (10), 1222–1233. https://doi.org/10.1061/(ASCE)1090-0241(2005)131:10(122.
[72] Moghal, A.A.B., Lateef, M.A., Mohammed, S.A.S., Lemboye, K., CS Chittoori, B., Almajed, A., 2020. Efficacy of enzymatically induced calcium carbonate precipitation in the retention of heavy metal ions. Sustainability 12 (17), 7019. https://doi.org/10.3390/su12177019.
[73] Mugwar, A.J., Harbottle, M.J., 2016. Toxicity effects on metal sequestration by microbially-induced carbonate precipitation. J Hazard Mater 314, 237–248. https://doi.org/10.1016/j.jhazmat.2016.04.039.
[74] Mwandira, W., Nakashima, K., Kawasaki, S., 2017. Bioremediation of lead-contaminated mine waste by Pararhodobacter sp. based on the microbially induced calcium carbonate precipitation technique and its effects on strength of coarse and fine grained sand. Ecol Eng 109, 57–64. https://doi.org/10.1016/j.ecoleng.2017.09.011.
[75] Okyay, T.O., Nguyen, H.N., Castro, S.L., Rodrigues, D.F., 2016. CO2 sequestration by ureolytic microbial consortia through microbially-induced calcite precipitation. Sci Total Environ 572, 671–680. https://doi.org/10.1016/j.scitotenv.2016.06.199.
[76] Okyay, T.O., Rodrigues, D.F., 2015. Biotic and abiotic effects on CO2 sequestration during microbially-induced calcium carbonate precipitation. p. fiv017 FEMS Microbiol Ecol 91 (3). https://doi.org/10.1093/femsec/fiv017.
[77] Petrie, S.E., Jackson, T.L., 1984. Effects of fertilization on soil solution pH and manganese concentration. Soil Sci Soc Am J 48 (2), 315–318. https://doi.org/10.2136/sssaj1984.03615995004800020018x.
[78] Proudfoot, D., Brooks, L., Gammons, C.H., Barth, E., Bless, D., Nagisetty, R.M., Lauchnor, E.G., 2022. Investigating the potential for microbially induced carbonate precipitation to treat mine waste. J Hazard Mater 424, 127490. https://doi.org/10.1016/j.jhazmat.2021.127490.
[79] Ptáček, P., Bartoníčková, E., Švec, J., Opravil, T., Šoukal, F., Frajkorová, F., 2015. The kinetics and mechanism of thermal decomposition of SrCO3 polymorphs. Ceram Int 41 (1), 115–126. https://doi.org/10.1016/j.ceramint.2014.08.043.
[80] Ptáček, P., Šoukal, F., Opravil, T., Havlica, J., Brandštetr, J., 2011. The kinetic analysis of the thermal decomposition of kaolinite by DTG technique. Powder Technol 208 (1), 20–25. https://doi.org/10.1016/j.powtec.2010.11.035.
[81] Qiao, S., Zeng, G., Wang, X., Dai, C., Sheng, M., Chen, Q., Xu, F., Xu, H., 2021. Multiple heavy metals immobilization based on microbially induced carbonate precipitation by ureolytic bacteria and the precipitation patterns exploration. Chemosphere 274, 129661. https://doi.org/10.1016/j.chemosphere.2021.129661.
[82] R Core Team (2022). R: A language and environment for statistical computing. R Foundation for Statistical Computing, Vienna, Austria. URL ⟨https://www.R-project.org/⟩.
[83] Railsback, L.B., 1999. Patterns in the compositions, properties, and geochemistry of carbonate minerals. Carbonates Evaporites 14 (1), 1–20. https://doi.org/10.1007/BF03176144.
[84] Reyes, I.A., Flores, M., Palacios, E.G., Islas, H., Juárez, J.C., Reyes, M., Teja, A.M., Pérez, C.A., 2020. Kinetics of the thermal decomposition of rhodochrosite. Minerals 11 (1), 34. https://doi.org/10.3390/min11010034.
[85] RStudio Team, 2020. RStudio: Integrated Development for R. RStudio. PBC, Boston, MA. ⟨http://www.rstudio.com/⟩ (URL).
[86] Sanyal, A., Rautaray, D., Bansal, V., Ahmad, A., Sastry, M., 2005. Heavy-metal remediation by a fungus as a means of production of lead and cadmium carbonate crystals. Langmuir 21 (16), 7220–7224. https://doi.org/10.1021/la047132g.
[87] Sardar, K., Ali, S., Hameed, S., Afzal, S., Fatima, S., Shakoor, M.B., Bharwana, S.A., Tauqeer, H.M., 2013. Heavy metals contamination and what are the impacts on living organisms. Greener. J Environ Manag Public Saf 2 (4), 172–179. https://doi.org/10.1016/j.jksus.2022.101865.
[88] Stocks-Fischer, S., Galinat, J.K., Bang, S.S., 1999. Microbiological precipitation of CaCO3. Soil Biol Biochem 31 (11), 1563–1571. https://doi.org/10.1016/S0038-0717(99)00082-6.
[89] Sumner, M.E., 1994. Measurement of soil pH: problems and solutions. Commun Soil Sci Plant Anal 25 (7-8), 859–879. https://doi.org/10.1080/00103629409369085.
[90] Tabatabai, M.A., 1977. Effects of trace elements on urease activity in soils. Soil Biol Biochem 9 (1), 9–13. https://doi.org/10.1016/0038-0717(77)90054-2.
[91] Tessier, A.P.G.C., Campbell, P.G., Bisson, M.J.A.C., 1979. Sequential extraction procedure for the speciation of particulate trace metals. Anal Chem 51 (7), 844–851. https://doi.org/10.1021/ac50043a017.
[92] Tkachenko, Y., Niedzielski, P., 2022. FTIR as a method for qualitative assessment of solid samples in geochemical research: a review. Molecules 27 (24), 8846. https://doi.org/10.3390/molecules27248846.
[93] UN, 2015. transforming our world: the 2030 agenda for sustainable development. Resolut Adopt Gen Assem 25 Sept 2015 42809, 1–13.
[94] Wang, L., Cheng, W.C., Xue, Z.F., Rahman, M.M., Xie, Y.X., 2024. Struvite and ethylenediaminedisuccinic acid (EDDS) enhance electrokinetic-biological permeable reactive barrier removal of copper and lead from contaminated loess. J Environ Manag 360, 121100. https://doi.org/10.1016/j.jenvman.2024.121100.
[95] Wickham, H., 2016. ggplot2: Elegant Graphics for Data Analysis. Springer-Verlag, New York.
[96] Xue, Z.F., Cheng, W.C., Rahman, M.M., Wang, L., Xie, Y.X., 2024. Immobilization of Pb (II) by Bacillus megaterium-based microbial-induced phosphate precipitation (MIPP) considering bacterial phosphorolysis ability and Ca-mediated alleviation of lead toxicity. Environ Pollut, 124229. https://doi.org/10.1016/j.envpol.2024.124229.
[97] Xue, Z.F., Cheng, W.C., Wang, L., Xie, Y.X., 2022. Catalyzing urea hydrolysis using two-step microbial-induced carbonate precipitation for copper immobilization: perspective of pH regulation. Front Microbiol 13, 1001464. https://doi.org/10.3389/fmicb.2022.1001464.
[98] Xue, Z.F., Cheng, W.C., Wang, L., Xie, Y.X., Qin, P., Shi, C., 2024. Immobilizing lead in aqueous solution and loess soil using microbially induced carbonate/phosphate precipitation (MICP/MIPP) under harsh pH environments. J Hazard Mater 480, 135884. https://doi.org/10.1016/j.jhazmat.2024.135884.
[99] Yang, J., Pan, X., Zhao, C., Mou, S., Achal, V., Al-Misned, F.A., Mortuza, M.G., Gadd, G.M., 2016. Bioimmobilization of heavy metals in acidic copper mine tailings soil. Geomicrobiol J 33 (3-4), 261–266. https://doi.org/10.1080/01490451.2015.1068889.
[100] Yin, T., Lin, H., Dong, Y., Wei, Z., Li, B., Liu, C., Chen, X., 2021. Inhibition of cadmium releasing from sulfide tailings into the environment by carbonate-mineralized bacteria. J Hazard Mater 419, 126479. https://doi.org/10.1016/j.jhazmat.2021.126479.
[101] Youseif, S.H., Abd El-Megeed, F.H., Humm, E.A., Maymon, M., Mohamed, A.H., Saleh, S.A., Hirsch, A.M., 2021. Comparative analysis of the cultured and total bacterial community in the wheat rhizosphere microbiome using culture-dependent and culture-independent approaches. Microbiol Spectr 9 (2), e00678-21. https://doi.org/10.1128/Spectrum.00678-21.
[102] Zambare, N.M., Naser, N.Y., Gerlach, R., Chang, C.B., 2020. Mineralogy of microbially induced calcium carbonate precipitates formed using single cell drop-based microfluidics. Sci Rep 10 (1), 17535. https://doi.org/10.1038/s41598-020-73870-y.
[103] Zelenková, G., Slovák, V., 2022. Decomposition of ammonium salts by quantitative TG-MS. J Therm Anal Calorim 147 (24), 15059–15068. https://doi.org/10.1007/s10973-022-11747-0.
[104] Zeng, Y., Chen, Z., Lyu, Q., Cheng, Y., Huan, C., Jiang, X., Yan, Z., Tan, Z., 2023. Microbiologically induced calcite precipitation for in situ stabilization of heavy metals contributes to land application of sewage sludge. J Hazard Mater 441, 129866. https://doi.org/10.1016/j.jhazmat.2022.129866.
[105] Zhao, X., Wang, M., Wang, H., Tang, D., Huang, J., Sun, Y., 2019. Study on the remediation of Cd pollution by the biomineralization of urease-producing

bacteria. Int J Environ Res Public Health 16 (2), 268. https://doi.org/10.3390/ijerph16020268.

[106] Zhao, Y., Yao, J., Yuan, Z., Wang, T., Zhang, Y., Wang, F., 2017. Bioremediation of Cd by strain GZ-22 isolated from mine soil based on biosorption and microbially induced carbonate precipitation. Environ Sci Pollut Res 24, 372–380. https://doi.org/10.1007/s11356-016-7810-y.

[107] Zhu, X., Li, W., Zhan, L., Huang, M., Zhang, Q., Achal, V., 2016. The large-scale process of microbial carbonate precipitation for nickel remediation from an industrial soil. Environ Pollut 219, 149–155. https://doi.org/10.1016/j.envpol.2016.10.047.